some pathway. But in the overexpression of full-length hVPS18, the SNK degradation is significantly enhanced. Our results suggest that hVPS18 regulates the protein level of SNK through its binding to the polo-domain and ubiquitylation of SNK. Activation of a number of protein kinases, such as protein kinase C (27), Src (28, 29), and ERK1/2 (30), results in ubiquitin/proteasome-mediated degradation that is dependent on their kinase activity. Taken together, SNK is regulated by the two fundamental intracellular mechanisms, phosphorylation and ubiquitin-dependent proteolysis, that control its kinase activity and molecular abundance.

Previous study revealed a functional role of SNK by establishing SNK-null mutant mice (18). Only growth retardation of embryo and slight delay of skeletal development of late gestation were reported as well as a delayed entry to S phase. Such mild phenotypes indicate that members of Plks may mutually compensate their function. Although it has not been clear how much hVPS18 contributes to the physiological protein level of SNK *in vivo*, the cell-cycle progression is similar between SNK−/− cells and HeLa cells overexpressing hVPS18. We assume that hVPS18 is involved in the degradation of SNK, at least in HeLa cells. In some cases, hVPS18 may not be the only E3 involved in SNK ubiquitylation, because the knock-down of hVPS18 did not completely abolish the ubiquitylation and degradation of SNK *in vivo* (data not shown). Several different classes of E3 ubiquitin ligases appear to directly regulate the same substrate in the case of p53, Numb, and Notch receptor (31, 32). For the ubiquitylation of Notch receptor, HECT type E3 ubiquitin ligase Suppressor of Deltex negatively regulates Notch through ubiquitylation (33). Meanwhile, its related Itch has been shown to ubiquitylate Notch 1 *in vivo* and *in vitro* (34). These lines of evidence suggest that the other pathway(s) for ubiquitylation of SNK may exist. Further analyses will be required to reveal the molecular mechanisms in detail.

Recently, Pak and Sheng (35) used the yeast-two hybrid screen to identify SNK as a new binding molecule for SPAR (spine-associated Rap guanosine triphosphatase (GTPase)-activating protein) that belongs to a growing list of post-synaptic proteins. The overexpression of SNK causes a depletion of SPAR and a loss of mature spines in hippocampal neurons. Biochemical analyses have shown that the neuronal activity induces the expression of SNK and that SNK phosphorylates SPAR (5). Together with our findings, the intracellular level of SNK protein plays a pivotal role not only in the regulation of cell-cycle progression, but also in the brain-specific functions such as learning and memory formation. Additional studies will be required to define further the precise mechanisms that control the protein level of SNK.

Acknowledgments—We greatly appreciate the help and support of Drs. Satoru Masuda, Keiji Wada, Eiki Kominami, Keiji Tanaka, and Yoshihisa Kudo. We thank members of the Dept. of Neurochemistry, NCNP, for discussion.

REFERENCES

1. Barr, F. A., Sillje, H. H., and Nigg, E. A. (2004) *Nat. Rev. Mol. Cell. Biol.* **5,** 429–440
2. Moshe, Y., Boulaire, J., Pagano, M., and Hershko, A. (2004) *Proc. Natl. Acad. Sci. U. S. A.* **101,** 7937–7942
3. Casenghi, M., Meraldi, P., Weinhart, U., Duncan, P. I., Korner, R., and Nigg, E. A. (2003) *Dev. Cell* **5,** 113–125
4. Jang, Y. J., Ma, S., Terada, Y., and Erikson, R. L. (2002) *J. Biol. Chem.* **277,** 44115–44120
5. Pak, D. T., and Sheng, M. (2003) *Science* **302,** 1368–1373
6. Kim, B. Y., Kramer, H., Yamamoto, A., Kominami, E., Kohsaka, S., and Akazawa, C. (2001) *J. Biol. Chem.* **276,** 29393–29402
7. Sato, T. K., Rehling, P., Peterson, M. R., and Emr, S. D. (2000) *Mol. Cell* **6,** 661–671
8. Hershko, A., and Ciechanover, A. (1998) *Annu. Rev. Biochem.* **67,** 425–479
9. Pickart, C. M. (2001) *Annu. Rev. Biochem.* **70,** 503–533
10. Schnell, J. D., and Hicke, L. (2003) *J. Biol. Chem.* **278,** 35857–35860
11. Freemont, P. S. (2000) *Curr. Biol.* **10,** R84–R87
12. Yogosawa, S., Miyauchi, Y., Honda, R., Tanaka, H., and Yasuda, H. (2003) *Biochem. Biophys. Res. Commun.* **302,** 869–872
13. Katayama, K., Wada, K., Miyoshi, H., Ohashi, K., Tachibana, M., Furuki, R., Mizuguchi, H., Hayakawa, T., Nakajima, A., Kadowaki, T., Tsutsumi, Y., Nakagawa, S., Kamisaki, Y., and Mayumi, T. (2004) *FEBS Lett.* **560,** 178–182
14. Simmons, D. L., Neel, B. G., Stevens, R., Evett, G., and Erikson, R. L. (1992) *Mol. Cell. Biol.* **12,** 4164–4169
15. Kauselmann, G., Weiler, M., Wulff, P., Jessberger, S., Konietzko, U., Scafidi, J., Staubli, U., Bereiter-Hahn, J., Strebhardt, K., and Kuhl, D. (1999) *EMBO J.* **18,** 5528–5539
16. Warnke, S., Kemmler, S., Hames, R. S., Tsai, H. L., Hoffmann-Rohrer, U., Fry, A. M., and Hoffmann, I. (2004) *Curr. Biol.* **14,** 1200–1207
17. Ma, S., Liu, M. A., Yuan, Y. L., and Erikson, R. L. (2003) *Mol. Cancer Res.* **1,** 376–384
18. Ma, S., Charron, J., and Erikson, R. L. (2003) *Mol. Cell. Biol.* **23,** 6936–6943
19. Glover, D. M., Ohkura, H., and Tavares, A. (1996) *J. Cell Biol.* **135,** 1681–1684
20. Elia, A. E., Rellos, P., Haire, L. F., Chao, J. W., Ivins, F. J., Hoepker, K., Mohammad, D., Cantley, L. C., Smerdon, S. J., and Yaffe, M. B. (2003) *Cell* **115,** 83–95
21. Cheng, K. Y., Lowe, E. D., Sinclair, J., Nigg, E. A., and Johnson, L. N. (2003) *EMBO J.* **22,** 5757–5768
22. Sevrioukov, E. A., He, J. P., Moghrabi, N., Sunio, A., and Kramer, H. (1999) *Mol. Cell* **4,** 479–486
23. Poupon, V., Stewart, A., Gray, S. R., Piper, R. C., and Luzio, J. P. (2003) *Mol. Bio. Cell* **14,** 4015–4027
24. Hamanaka, R., Maloid, S., Smith, M. R., O'Connell, C. D., Longo, D. L., and Ferris, D. K. (1994) *Cell Growth Differ.* **5,** 249–257
25. Elia, A. E., Cantley, L. C., and Yaffe, M. B. (2003) *Science* **299,** 1228–1231
26. Jang, Y. J., Lin, C. Y., Ma, S., and Erikson, R. L. (2002) *Proc. Natl. Acad. Sci. U. S. A.* **99,** 1984–1989
27. Lu, Z., Liu, D., Hornia, A., Devonish, W., Pagano, M., and Foster, D. A. (1998) *Mol. Cell. Biol.* **18,** 839–845
28. Hakak, Y., and Martin, G. S. (1999) *Curr. Biol.* **9,** 1039–1042
29. Harris, K. F., Shoji, I., Cooper, E. M., Kumar, S., Oda, H., and Howley, P. M. (1999) *Proc. Natl. Acad. Sci. U. S. A.* **96,** 13738–13743
30. Lu, Z., Xu, S., Joazeiro, C., Cobb, M. H., and Hunter, T. (2002) *Mol. Cell* **9,** 945–956
31. Nie, J., McGill, M. A., Dermer, M., Dho, S. E., Wolting, C. D., and McGlade, C. J. (2002) *EMBO J.* **21,** 93–102
32. Susini, L., Passer, B. J., Amzallag-Elbaz, N., Juven-Gershon, T., Prieur, S., Privat, N., Tuynder, M., Gendron, M. C., Israel, A., Amson, R., Oren, M., and Telerman, A. (2001) *Proc. Natl. Acad. Sci. U. S. A.* **98,** 15067–15072
33. Cornell, M., Evans, D. A., Mann, R., Fostier, M., Flasza, M., Monthatong, M., Artavanis-Tsakonas, S., and Baron, M. (1999) *Genetics* **152,** 567–576
34. Qiu, L., Joazeiro, C., Fang, N., Wang, H. Y., Elly, C., Altman, Y., Fang, D., Hunter, T., and Liu, Y. C. (2000) *J. Biol. Chem.* **275,** 35734–35737
35. Pak, D. T., Yang, S., Rudolph-Correia, S., Kim, E., and Sheng, M. (2001) *Neuron* **31,** 289–303

Ubiquitin C-terminal hydrolase L1 regulates the morphology of neural progenitor cells and modulates their differentiation

Mikako Sakurai[1,2], Koichi Ayukawa[1], Rieko Setsuie[1,2], Kaori Nishikawa[1], Yoko Hara[1], Hiroki Ohashi[1,3], Mika Nishimoto[1,4], Toshiaki Abe[3], Yoshihisa Kudo[4], Masayuki Sekiguchi[1], Yae Sato[1,2], Shunsuke Aoki[1], Mami Noda[2] and Keiji Wada[1,*]

[1]Department of Degenerative Neurological Diseases, National Institute of Neuroscience, National Center of Neurology and Psychiatry, Kodaira, Tokyo, 187-8502, Japan
[2]Laboratory of Pathophysiology, Graduate School of Pharmaceutical Sciences, Kyushu University, Higashi-ku, Fukuoka, 812-8582, Japan
[3]Department of Neurosurgery, Graduate School of Medicine, Jikei University School of Medicine, Minato-ku, Tokyo, 105-8461, Japan
[4]Laboratory of Cellular Neurobiology, Tokyo University of Pharmacy and Life Science, Hachioji, Tokyo, 192-0392, Japan
*Author for correspondence (e-mail: wada@ncnp.go.jp)

Accepted 27 September 2005
Journal of Cell Science 119, 162-171 Published by The Company of Biologists 2006
doi:10.1242/jcs.02716

Summary

Ubiquitin C-terminal hydrolase L1 (UCH-L1) is a component of the ubiquitin system, which has a fundamental role in regulating various biological activities. However, the functional role of the ubiquitin system in neurogenesis is not known. Here we show that UCH-L1 regulates the morphology of neural progenitor cells (NPCs) and mediates neurogenesis. UCH-L1 was expressed in cultured NPCs as well as in embryonic brain. Its expression pattern in the ventricular zone (VZ) changed between embryonic day (E) 14 and E16, which corresponds to the transition from neurogenesis to gliogenesis. At E14, UCH-L1 was highly expressed in the ventricular zone, where neurogenesis actively occurs; whereas its expression was prominent in the cortical plate at E16. UCH-L1 was very weakly detected in the VZ at E16, which corresponds to the start of gliogenesis. In cultured proliferating NPCs, UCH-L1 was co-expressed with nestin, a marker of undifferentiated cells. In differentiating cells, UCH-L1 was highly co-expressed with the early neuronal marker TuJ1. Furthermore, when UCH-L1 was induced in nestin-positive progenitor cells, the number and length of cellular processes of the progenitors decreased, suggesting that the progenitor cells were differentiating. In addition, NPCs derived from *gad* (UCH-L1-deficient) mice had longer processes compared with controls. The ability of UCH-L1 to regulate the morphology of nestin-positive progenitors was dependent on its binding affinity for ubiquitin but not on hydrolase activity; this result was also confirmed using *gad*-mouse-derived NPCs. These results suggest that UCH-L1 spatially mediates and enhances neurogenesis in the embryonic brain by regulating progenitor cell morphology.

Key words: PGP9.5, UCH-L1, Nestin, Ubiquitin, Cell morphology, Differentiation, Progenitor

Introduction

Ubiquitin C-terminal hydrolase L1 (UCH-L1) is a member of the deubiquitylating enzymes and is one of the most abundant proteins in the brain. Whereas other UCH members are ubiquitously expressed, UCH-L1 is selectively expressed in neurons and testes/ovaries in the adult (Wilkinson et al., 1989). UCH-L1 is also known as PGP9.5 and is used as a neuron-specific marker in neuroanatomical and neuropathological studies (Dickson et al., 1994; McQuaid et al., 1995). Recent studies suggest that UCH-L1 is involved in neurodegeneration. The I93M mutation and the S18Y polymorphism in UCH-L1 are implicated in Parkinson's disease (Leroy et al., 1998; Satoh and Kuroda, 2001). Using gracile axonal dystrophy (*gad*) mice, we previously demonstrated that the dying-back type of axonal degeneration is caused by a deletion of the *Uchl1* gene (Saigoh et al., 1999). UCH-L1 has an affinity for ubiquitin and ensures its stability within neurons in vivo (Osaka et al., 2003). Furthermore, UCH-L1 has ubiquitin ligase activity (Liu et al., 2002). Thus, UCH-L1 might have multiple functions and more roles in biological phenomena than previously expected.

UCH-L1 mRNA is first detected at embryonic day (E) 8.5-9 in the neural tube and in the neural epithelium (Schofield et al., 1995). In addition, UCH-L1 immunoreactivity has been observed in the neural tube at E10.5 (Sekiguchi et al., 2003). However, its functional role in embryonic neurogenesis is not well understood. CDK5 and Dab1 are involved in regulating the migratory behavior of postmitotic neurons. Both p35, which is a CDK5 kinase, and Dab1 are degraded by the ubiquitin-proteasome pathway (Arnaud et al., 2003; Bock et al., 2004; Patrick et al., 1998). Thus, the ubiquitin system might be important in the migration and differentiation of postmitotic neurons and for the lamination pattern of the cerebral cortex.

Neural progenitor cells (NPCs) differentiate into neurons, astrocytes and oligodendrocytes (Qian et al., 1998; Qian et al., 2000; Shen et al., 1998). In the embryonic brain, neuroepithelial cells and radial glia are present in the ventricular zone (VZ); neurogenesis occurs first, followed by

gliogenesis. Committed progenitor cells move from the VZ to the cortical plate (CP) (Noctor et al., 2004). The differentiating cells migrate by means of radial migration, during which the migrating cells change their morphology (Kawauchi et al., 2003; Noctor et al., 2002; Tabata and Nakajima, 2003). Here, we analyzed the functional role of UCH-L1 using mouse embryonic NPCs. Our results indicate that UCH-L1 is expressed in nestin-positive NPCs and might regulate neurogenesis. The expression pattern of UCH-L1 changed in parallel with the transition from neuronal generation to glial generation. Furthermore, UCH-L1 modulated the length of nestin-positive processes in NPCs. Our results constitute the first evidence that UCH-L1 is important in neurogenesis and thus provide the basis for further investigation into the role of the ubiquitin system in neurogenesis.

Results

UCH-L1 expression in embryonic mouse brain

We first determined the specificity of the UCH-L1 antibody using immunoblotting (data not shown) and immunostaining. Because *gad* mice do not express endogenous UCH-L1 (Saigoh et al., 1999), we used these mice as a negative control. Heterozygous littermates had UCH-L1 immunostaining, whereas UCH-L1 immunoreactivity was not detected in the brains of *gad* mice (Fig. 1). These results confirmed the specificity of the antibody against UCH-L1. Using this antibody, we further compared the distribution and expression of UCH-L1 with the neural progenitor marker nestin and the early neuronal marker TuJ1. Nestin was expressed in the VZ of brains from both *gad* and heterozygous mice at E13 (Fig. 1). Nestin expression was observed throughout the region, whereas TuJ1 immunoreactivity was detected at the marginal zone (MZ). In heterozygous mice, UCH-L1 and nestin immunostaining overlapped in almost all cells in the VZ, suggesting that UCH-L1 is expressed in NPCs (Fig. 1A). TuJ1 expression colocalized with that of UCH-L1 in MZ cells, indicating that UCH-L1 is expressed in embryonic neurons as well (Fig. 1B). In E13 *gad* mouse brain, nestin staining differed compared with that in heterozygous littermates. Nestin staining was observed in many long radial fibers in the mutant, which we believed were radial glia; by contrast, staining in the heterozygotes occurred in radial glia as well as in neuronal cells at various stages of development (Fig. 1A; arrow and arrowhead).

We then looked for developmental changes in UCH-L1 expression. In the embryonic cerebral cortex, asymmetric cell division generates one neuron and one neural progenitor (Roegiers and Jan, 2004; Zhong et al., 1996; Zhong et al., 1997). These asymmetric cell divisions begin at E11, peak around E14, and subside after E16. At E14, astrocytes and oligodendrocytes are not yet present. However, at E16, glial cell production begins. The regional expression level for both nestin and TuJ1 did not change between E14 and E16 (Fig. 2A,B). At E14 and E16, nestin immunoreactivity was stronger in the VZ (Fig. 2A) and was faintly detected only along radial glial fibers in the CP (Fig. 2A,C; arrowhead) (Malatesta et al., 2003; Malatesta et al., 2000). TuJ1 immunoreactivity was predominantly detected in the MZ, CP, intermediate zone and subventricular zone at E14 and E16 (Fig. 2B,D). In the VZ, TuJ1 immunoreactivity was detected only in migrating neurons (Fig. 2D; arrowhead).

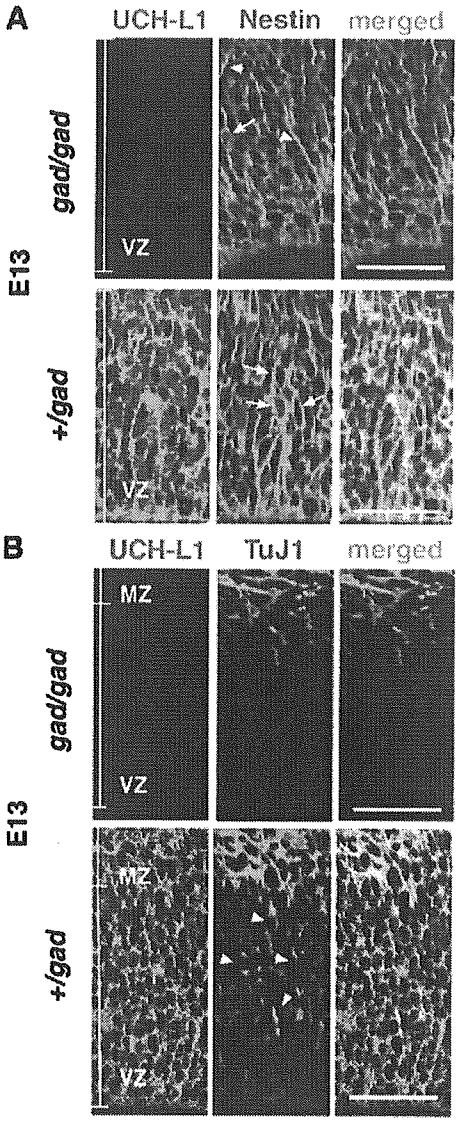

Fig. 1. Antibody specificity and expression of UCH-L1 in the ventricular zone at E13. UCH-L1 expression was detected using immunohistochemistry with anti-PGP9.5. UCH-L1 is not detected in the brain of *gad* mice at E13 (A,B) but is strongly expressed in heterozygous littermates (A,B). Confocal microscopic images of coronal sections of *gad* mice and heterozygous littermates were double stained with antibodies for the progenitor marker nestin and UCH-L1 (PGP9.5) (A) or for the early neuronal marker tubulin β III (TuJ1) and UCH-L1 (B). Long radial fibers are indicated by arrowheads, and various phases of progenitor cells are indicated by arrows (A). TuJ1-positive, migrating neuronal cells are indicated by arrowheads (B). MZ, marginal zone; VZ, ventricular zone. Bars, 40 μm.

By contrast, the pattern of UCH-L1 expression changed between E14 and E16 (Fig. 2A,B). At both stages of development, UCH-L1 was expressed in neuronal cells as well as in progenitor cells. UCH-L1 immunoreactivity was stronger in the VZ than in the CP at E14; however, the immunoreactivity

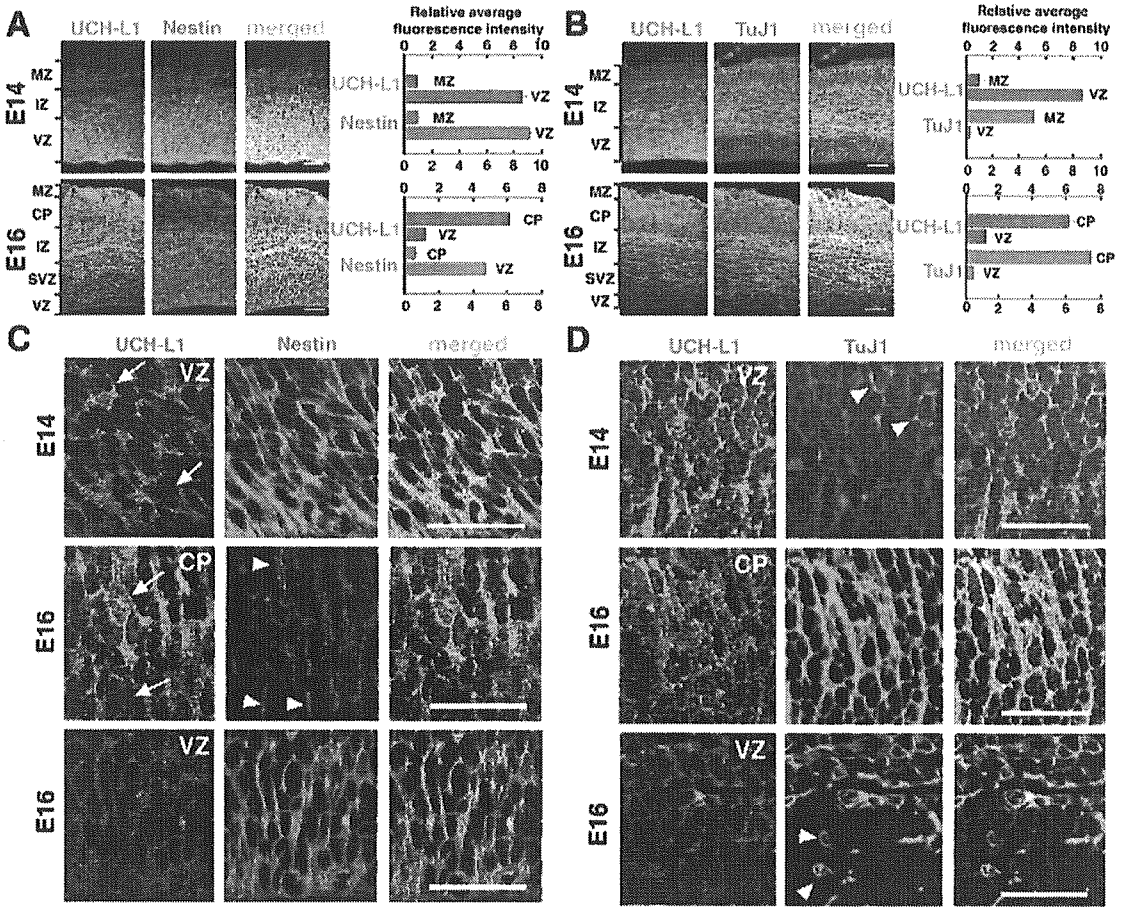

Fig. 2. Change in UCH-L1 expression pattern in the developing mouse brain. Cryosections of the brain at E14 and E16 were double stained with UCH-L1 and the neural progenitor marker nestin (A) or early neuronal marker TuJ1 (B). Unlike with UCH-L1, staining patterns for TuJ1 and nestin do not change between E14 and E16. At E14, UCH-L1 expression is higher in the VZ than in the MZ. At E16, higher expression of UCH-L1 is reciprocally detected in the CP. By contrast, at both E14 and E16, nestin is highly expressed in the VZ, and TuJ1 expression is higher in the MZ/CP. Fluorescence intensities per field (1700 μm^2) were measured in each layer of the E14 and E16 brain and are shown to the right. Bars, 80 μm. (C,D) Higher-magnification images from A,B of UCH-L1 expression in the E14 and E16 brain: UCH-L1 and nestin (C); UCH-L1 and TuJ1 (D). UCH-L1 and nestin are co-expressed in the VZ at E14 and E16. Nestin is expressed only in radial glial fibers (arrowheads) of the CP but not in neurons. UCH-L1 expression level is high. A representative cell with a high level of UCH-LI expression is indicated by a white arrow and one with low expression is indicated by a yellow arrow (C). An early neuronal marker, TuJ1, was expressed in both migrating (arrowheads) and mature neurons (D). CP, cortical plate; IZ, intermediate zone; MZ, marginal zone; SVZ, subventricular zone; VZ, ventricular zone. Bars, 40 μm.

was stronger in the CP than in the VZ at E16 (Fig. 2A,B). The regional change in UCH-L1 expression between E14 and E16 was further confirmed by measuring immunofluorescence intensities from confocal images of the MZ/CP and VZ. At E14, the relative UCH-L1 expression level in the VZ was 9.3 times higher than that in the MZ (Fig. 2A).

Conversely, at E16, when neuronal maturation occurs in the CP, UCH-L1 immunoreactivity in the CP was 5.0 times higher than in the VZ (Fig. 2B). UCH-L1 immunoreactivity colocalized with that of nestin in the VZ at both E14 and E16, although UCH-L1 expression in the VZ was lower at E16 (Fig. 2C). In the VZ at E14, nestin was expressed homogeneously; however, the pattern of UCH-L1 immunoreactivity was mixed, with strong and weak intensities (Fig. 2C; arrow). This expression pattern might reflect the heterogeneity of progenitor cells. Nestin-positive radial glial fibers were observed in the CP at E16 through mature neurons, which strongly expressed UCH-L1 (Fig. 2C) (Malatesta et al., 2000; Malatesta et al., 2003).

UCH-L1 and nestin expression in cultured NPCs

Because areas of nestin and UCH-L1 immunoreactivity overlapped in the VZ, where NPCs reside, we subsequently analyzed the transition of UCH-L1 expression using cultured NPCs. We performed double-labeling experiments for UCH-L1 and nestin expression in cultured NPCs. In the presence of basic fibroblast growth factor (bFGF), when NPCs are proliferating, the percentage of UCH-L1/nestin double-positive

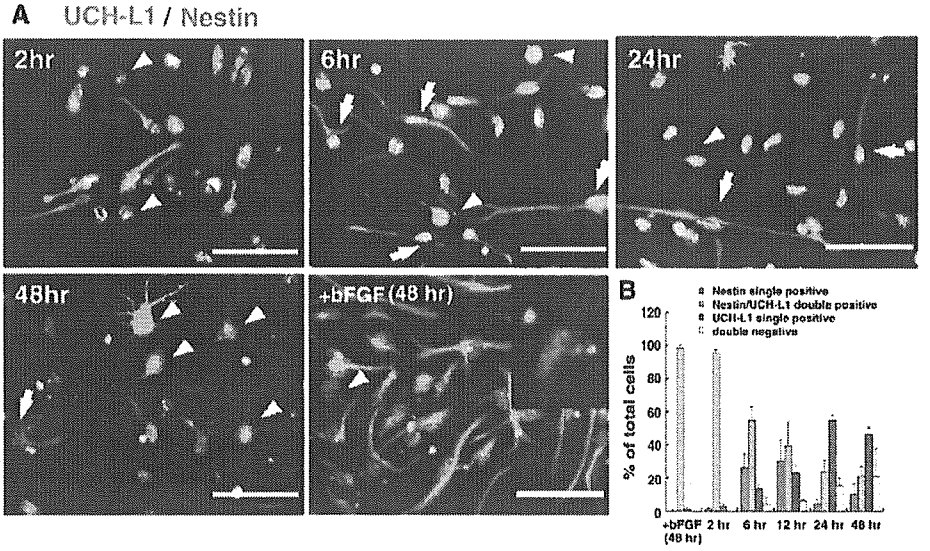

Fig. 3. Nestin and UCH-L1 expression in undifferentiated and differentiating NPCs at 2, 6, 12, 24 and 48 hours. (A) NPCs were immunolabeled with antibodies against nestin and UCH-L1 in the proliferating phase (+bFGF; at 48 hours) or the differentiation phase (–bFGF; 2, 6, 24, 48 hours). Cultures were counterlabeled with Hoechst nuclear dye to facilitate cell quantification. (B) Quantitative analysis of the percentage of cells stained with each antibody. Nestin-positive cells gradually decrease as differentiation proceeds. The UCH-L1 expression level is both high (arrowheads) and low (arrows) in nestin-positive cells at 6 hours. Each experiment was analyzed by counting cells in three independent wells at the indicated times. The experiments were repeated at least two times. Bars, 50 μm.

cells did not change 48 hours after plating, and almost all NPCs expressed UCH-L1 (Fig. 3A). The majority (97.5±2.2%; mean±s.d.) of cultured cells were nestin positive and most of them also stained for UCH-L1 2 hours after plating without bFGF, which triggers NPC differentiation. UCH-L1/nestin double-positive cells were detected at all time points, but as differentiation proceeded their numbers gradually decreased from 95.8±1.9% at 2 hours to 21.5±5.8% at 48 hours (Fig. 3A,B). Although UCH-L1 single-positive cells were rarely detected at 2 hours, the population increased with differentiation, and by 24 hours after bFGF removal 55.1±2.9% of cultured cells were UCH-L1 single-positive cells. Conversely, nestin single-positive cells were readily detected during the earlier phase of differentiation, especially at 6 hours (26.4±8.4% of total cells) and 12 hours (27.0±14.0% of total cells). The differentiating NPCs included nestin-positive cells in which UCH-L1 was either strongly or weakly expressed (Fig. 3A; arrow and arrowhead at 6 hours). These data indicate that UCH-L1 is expressed in progenitor cells as well as in differentiating NPCs. Nestin-positive cells can probably be

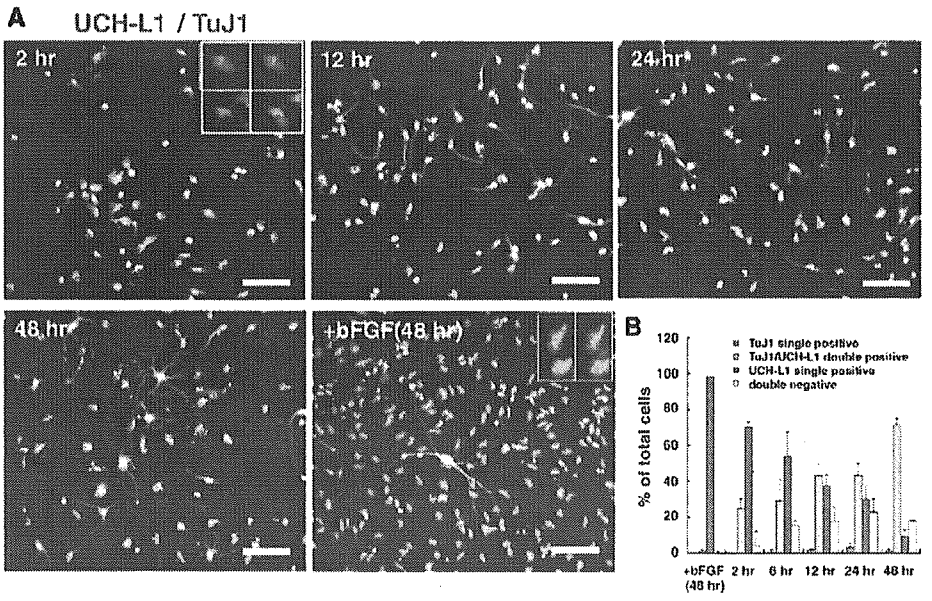

Fig. 4. UCH-L1 expression in neurogenesis. NPCs were immunolabeled with antibodies against TuJ1 and UCH-L1. Cultures were counterlabeled with Hoechst nuclear dye to facilitate cell quantification. Quantitative analysis of the percentage of cells stained with each antibody. (A) In the proliferating phase (+bFGF; at 48 hours) or the differentiation phase (–bFGF; 2, 12, 24, 48 hours), most TuJ1-positive cells co-express UCH-L1. The UCH-L1 expression level is both high and low in TuJ1-positive cells at 48 hours. (B) Quantitative analysis of the percentage of cells stained with each antibody. The number of TuJ1-positive cells gradually increased in the differentiating phase (–bFGF; B). Each experiment was analyzed by counting cells in three independent wells at the indicated times. The experiments were repeated at least two times. Bars, 50 μm.

categorized into at least two subgroups based on their UCH-L1 expression (Fig. 3A,B).

UCH-L1 and TuJ1 expression in cultured NPCs

We then analyzed the expression patterns of UCH-L1 and TuJ1. In the presence of bFGF, TuJ1-positive cells were rarely detected. However, in the absence of bFGF, TuJ1-positive cells were induced. In the cultures without bFGF, as the UCH-L1 single-positive cell population decreased with time, the UCH-L1/TuJ1 double-positive population increased (Fig. 4A,B). UCH-L1/TuJ1 double-negative cells were detected in the differentiating phases at 6, 12, 24 and 48 hours. UCH-L1/TuJ1 double-negative cells might be the nestin single-positive cells at 6 hours and 12 hours in Figs 3 and 4. TuJ1 single-positive cells were infrequently detected in the differentiating NPCs. Because 71.4±3.4% of NPCs differentiated into TuJ1-positive cells under our culture conditions without bFGF at 48 hours, almost all UCH-L1-positive cells are thought to differentiate into TuJ1-positive neuronal cells (Fig. 4A,B). The differentiating NPCs included TuJ1-positive cells in which UCH-L1 was either strongly or weakly expressed (Fig. 4A). These data indicate that UCH-L1-positive NPCs have a high potential for differentiating into neuronal cells and that TuJ1-positive neuronal cells are heterogeneous with regard to UCH-L1 expression.

Morphological classification of UCH-L1-positive NPCs

Nestin is a marker of undifferentiated cells, whereas UCH-L1 is a neuron-specific marker. Here, UCH-L1/nestin double-positive cells were present in cultured NPCs as well as in embryonic brain (Figs 2, 3). Cultured NPCs sequentially gave rise to neurons, then astrocytes, and finally oligodendrocytes (data not shown). Under our culture conditions, neurogenesis actively occurred in differentiating NPCs between 2 and 12 hours after plating (Fig. 4). Glial differentiation had not begun by this time. We collected differentiating NPCs at 6 hours and 12 hours after plating and then analyzed the morphology of nestin-positive cells (Fig. 5). Both UCH-L1/nestin double-positive cells and nestin single-positive cells were present in the population of differentiating NPCs. As the population of double-positive cells might represent a progression of differentiating neurons, we examined the morphology of these cells. Differentiating neurons undergo a stereotypical set of morphological changes, including length (from long to short) (Fukuda et al., 2003; Hartfuss et al., 2003; Nadarajah et al., 2001). We categorized the nestin-positive cells with respect to process length (long, short or round; Fig. 3). UCH-L1 single-positive and double-negative cells were included in the total number of cells. When the total length of processes was more than four times the diameter of the nucleus of the cell, the cell was categorized as 'long', whereas cells with shorter processes were categorized as 'short'. Cells that did not have processes were classified as 'round'. At 6 hours, the majority of nestin single-positive cells were long (18.2±7.6% vs 4.0±0.2% short cells; mean±s.d.; Fisher's PLSD, P=0.008), whereas the majority of UCH-L1/nestin double-positive cells were short (62.0±6.3%). This population was significantly greater than that of long cells (10.3±2.0%) and round cells (5.0±1.7%; Fisher's PLSD, P<0.0001). When NPCs with processes were subcategorized as unipolar, bipolar or multipolar, the unipolar population was significantly higher (62.3±16.9%) than the bipolar population (18.2±3.9%; Fisher's PLSD, P=0.002) in UCH-L1/nestin double-positive cells. Multipolar cells were not observed at 12 hours. However, in nestin single-positive cells, more NPCs were bipolar (16.5±4.6%) than unipolar (4.5±1.9%; Fisher's PLSD, P=0.009; Fig. 6B). Similar results were obtained at 12 hours (Fig. 6). Thus, most UCH-L1/nestin double-positive cells had shorter processes and were more likely to be unipolar.

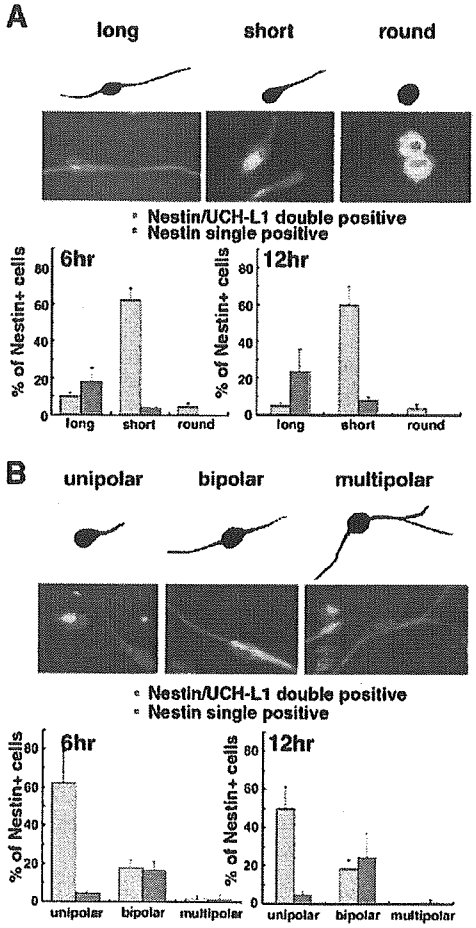

Fig. 5. Morphological identification of subpopulations of cultured NPCs at 6 and 12 hours after induction of differentiation. Differentiating NPCs were double stained with UCH-L1 and nestin. For the quantification depicted in A, differentiating NPCs stained with UCH-L1 and nestin were classified as long, short or round (see text). For the quantification depicted in B, differentiating NPCs were classified based on three kinds of cell morphology: unipolar, bipolar, or multipolar.

Effect of UCH-L1 on nestin-positive processes

We next examined the effect of UCH-L1 on proliferating NPC morphology using the transient transfection method. NPCs were allowed to proliferate for 48 hours after transfection and were then induced to differentiate for 12 hours. The cells were fixed, and the length of nestin-positive processes was examined. To quantify the relationship between UCH-L1 expression and process formation, we measured the total length

of nestin-positive processes. Untransfected NPCs that were nestin positive had mainly long, bipolar processes (Fig. 3A, +bFGF). Cells that were transfected with a green fluorescent protein (GFP) expression vector (negative control) had a morphology that was similar to that of untransfected cells (Fig. 6A). By contrast, cells transfected with wild-type (WT) UCH-L1 cDNA had significantly shorter processes (47.6±6.4 μm, mean±s.e.m., n=81) than mock-transfected cells (69.9±7.0 μm, n=82) (Fig. 6A).

We then examined the relationship between the UCH-L1 structure and its activity with respect to morphological induction. We prepared two UCH-L1 mutants: D30A UCH-L1 lacked hydrolase activity and binding affinity for ubiquitin (Fig. 6B,C) (Osaka et al., 2003); C90S UCH-L1 lacked hydrolase activity but maintained binding affinity for ubiquitin (Fig. 6B,C) (Osaka et al., 2003). We compared the deubiquitylating activity of each UCH-L1 mutant using Ub-AMC as a substrate. The D30A mutant had little hydrolase activity, and the activity of the C90S mutant was not detectable (Fig. 6B; right). Sodium dodecyl sulfate-polyacrylamide gel electrophoresis revealed that there were no detectable contaminating proteins in these recombinant protein preparations (Fig. 6B; left). Co-immunoprecipitation experiments demonstrated that WT UCH-L1 and the C90S mutant physically associated with monoubiquitin. The D30A mutant (as well as GFP alone, which was used as a control) did not associate with ubiquitin (Fig. 6C). Although we did not detect a statistically significant difference, cells transfected with the D30A mutant tended to have longer nestin-positive processes (83.4±7.1 μm, n=87) as compared with cells transfected with the GFP expression vector (Fig. 6A). By contrast, cells transfected with the C90S mutant had significantly shorter fibers (39.3±4.5 μm, n=120; ANOVA: F=11.5, P<0.0001; Dunnett's multiple comparison test: GFP vs WT, P<0.05; GFP vs C90S, P<0.001; GFP vs D30A, P>0.05; Fig. 6A). We also compared the length of nestin-positive processes among UCH-L1 mutants (Bonferroni-Dunn Multiple Comparison Test: WT vs C90S, P=0.32; WT vs D30A, P<0.0001; D30A vs C90S, P<0.0001). Taken together, our data suggest that the effect of UCH-L1 expression on NPC morphology is dependent on the interaction between monoubiquitin and UCH-L1.

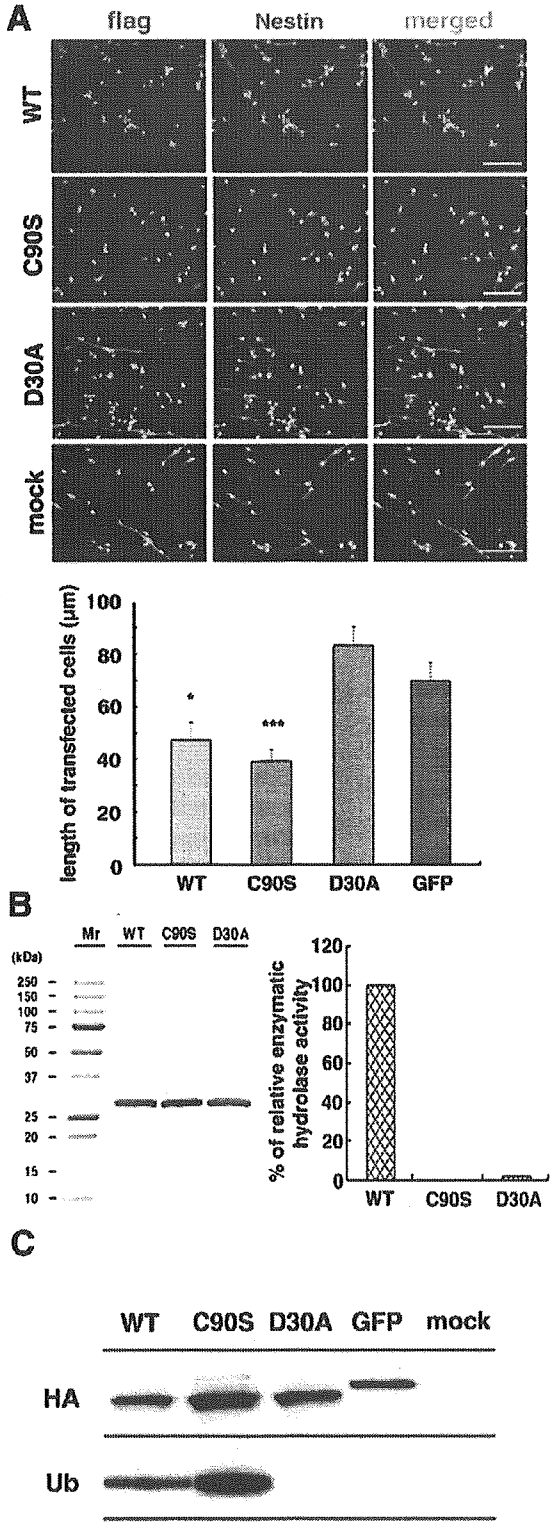

Fig. 6. The induction of short processes depends on the interaction between UCH-L1 and monoubiquitin. (A) FLAG-tagged WT UCH-L1, C90S UCH-L1, D30A UCH-L1 and GFP (all in the pCI-*neo* vector) were transfected into NPCs. Antibodies against the FLAG-tag were used to detect transfected UCH-L1. The green staining shows transfected cells and the red staining shows endogenous nestin. Transient transfection of each construct was performed under proliferating conditions. At 48 hours after transfection, bFGF was removed for 12 hours before the cultures were immunostained. The lengths of nestin-positive processes in immunostained cells were measured. Asterisks indicate differences from the value of GFP-transfected NPCs at *P<0.05 and ***P<0.001. Bars, 80 μm. (B) Visualization of recombinant 6HN-tagged UCH-L1 by sodium dodecyl sulfate-polyacrylamide gel electrophoresis with Coomassie staining (B, left). UCH-L1 hydrolase activity was measured by Ub-AMC hydrolysis. Enzyme concentration was 4.3 nM, and substrate concentration was 700 nM. Initial velocity data was used to determine the values for relative hydrolase activity of UCH-L1 (B, right). (C) UCH-L1 co-immunoprecipitated with Ub. Cytosolic extracts from NIH-3T3 cell lines stably expressing HA-tagged WT UCH-L1 and mutants thereof were immunoprecipitated using anti-HA and immunoblotted with anti-HA antibody or anti-Ub antibody.

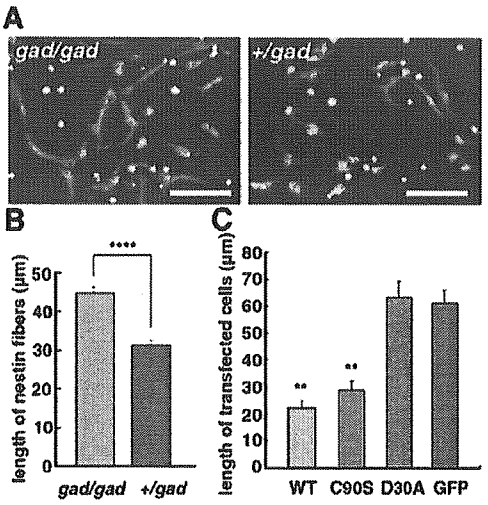

Fig. 7. A comparative experiment of *gad* mice and heterozygous littermates. The experiment compared *gad* mice (A,B) with a transfection study using FLAG-tagged WT UCH-L1, C90S UCH-L1, D30A UCH-L1 and GFP (mock) into *gad*-mouse-derived NPCs (C). The lengths of nestin-positive processes in immunostained cells were measured. NPCs from *gad* mice had longer nestin-positive processes compared with the control (A,B). (C) At 48 hours after transfection, bFGF was removed for 12 hours before the cultures were immunostained. The lengths of nestin-positive processes in immunostained cells were measured. Asterisks indicate differences from the value of GFP-transfected NPCs at $^{**}P<0.01$ and $^{****}P<0.0001$. Bar, 50 μm.

A comparative experiment using *gad*-mouse-derived NPCs

We did a comparative experiment using *gad* mice and heterozygous littermates. Nestin-positive NPCs from *gad* mice had longer processes. When we measured the length of nestin-positive fibers, NPCs from *gad* mice (45.0±1.4 μm, mean±s.e.m., n=366) had significantly longer nestin-positive processes compared with the control (31.4±1.3 μm, n=363) (Mann-Whitney U test: *gad* vs control, $P<0.0001$; Fig. 7A,B).

We next examined the effect of UCH-L1 on *gad*-mouse-derived NPCs using the transient transfection method. As observed in B6-derived cells, NPCs from *gad* mice that were transfected with WT UCH-L1 cDNA had significantly shorter processes (22.2±2.7 μm, mean±s.e.m., n=70) than mock-transfected cells (61.0±4.9 μm, n=88) (Bonferroni-Dunn multiple comparison test: GFP vs WT, $P<0.0001$) (Fig. 7C). Similarly, cells transfected with the C90S mutant had significantly shorter fibers (28.9±3.1 μm, n=71) (GFP vs C90S, $P<0.0001$). Although we did not detect a statistically significant difference, cells transfected with the D30A mutant tended to have longer nestin-positive processes (63.3±5.9 μm, n=80) as compared with cells transfected with the GFP expression vector (GFP vs D30A, P=0.70) (Fig. 7C). We also compared the length of nestin-positive processes among UCH-L1 mutants (Bonferroni-Dunn multiple comparison test: WT vs C90S, P=0.32; WT vs D30A, $P<0.0001$; D30A vs C90S, $P<0.0001$). Taken together, our data suggest that the effect of UCH-L1 expression on NPC morphology is dependent on the interaction between monoubiquitin and UCH-L1.

Discussion

UCH-L1 is a neuron-specific marker in the adult brain. In the present study, we provide experimental evidence that UCH-L1 is expressed in NPCs (Figs 2, 3). Using immunohistochemistry in the mouse brain, we detected UCH-L1 expression at E14 and E16. Interestingly, the expression pattern differed between E14 and E16 (Fig. 2). At E14, when the CP is forming, UCH-L1 expression was higher in the VZ than in the CP. At E14, the VZ contains progenitor cells that are generating neurons in the neocortex (Hashimoto and Mikoshiba, 2004; Malatesta et al., 2003). By contrast, UCH-L1 expression at E16 was lower in the VZ than in the CP. At E16, neuritogenesis and neuronal maturation are active in the CP, and gliogenesis is beginning in the VZ (Rice and Curran, 2001). The cerebral cortex layer becomes thicker at E16, where glial cells are not yet generated. The staining pattern for TuJ1 and nestin did not change between E14 and E16 (Fig. 2), indicating that UCH-L1 is highly expressed in the cortical layer prior to gliogenesis. The change in the expression pattern of UCH-L1 was coincident with the transition from neurogenesis to gliogenesis in the VZ. These results raise the possibility that UCH-L1 mediates not only the neuronal differentiation of NPCs but also the transition from neurogenesis to gliogenesis.

Time is a pivotal factor in the programmed sequence that produces neurons and glial cells from NPCs (Qian et al., 2000), in that the switch from neurogenesis to gliogenesis is regulated by time. The mechanism behind this progression of the progenitor cells is not well understood. Cultured NPCs generate neurons first, followed by astrocytes and then oligodendrocytes (Qian et al., 2000; Temple, 2001). This order of production for each population has been verified in vivo (Sauvageot and Stiles, 2002). The pattern of UCH-L1 immunoreactivity suggests that UCH-L1 is required for the onset of neurogenesis, which is followed by glial differentiation (Fig. 2).

We thus examined the role of UCH-L1 in neurogenesis using cultured NPCs. In UCH-L1/nestin double-staining experiments, the number of double-positive cells decreased with time in culture (Fig. 3). Conversely, UCH-L1 single-positive cells increased. In the double-staining experiments for UCH-L1 and TuJ1, the number of UCH-L1 single-positive cells decreased with time in culture, whereas the number of UCH-L1/TuJ1 double-positive cells increased (Fig. 4). These observations suggest that most UCH-L1-positive cells initially express nestin, but they express TuJ1 at a later stage. As we observed in vivo and in vitro (Figs 2-4), NPCs express UCH-L1, and its expression increases as the NPCs differentiate into neuronal cells. The number of nestin single-positive cells transiently increased before the UCH-L1 single-positive population increased (Fig. 3). The nestin single-positive population might have changed into the UCH-L1/nestin double-negative population (Fig. 3). Although the fate of the double-negative populations remains unknown, the double-negative cells might represent glial cells. Alternatively, some of the nestin single-positive cells might have changed into UCH-L1/nestin double-positive cells and then differentiated into UCH-L1 single-positive cells. A few UCH-L1-negative and TuJ1-positive cells were detected in the differentiating NPCs (Fig. 4). Thus, TuJ1-positive early neurons appear to be heterogeneous. UCH-L1/TuJ1 double-positive immunoreactivity suggested that UCH-L1 is not

absolutely required for some portion of neuronal cell development (Fig. 1B and Fig. 4A). This might explain why *gad* mouse neurons develop despite the absence of UCH-L1.

Because UCH-L1 was expressed in nestin-positive NPCs, we further examined the role of UCH-L1 in cell morphology (Fig. 5). Differentiating NPCs change morphology (Noctor et al., 2001), but the role of UCH-L1 in differentiating neurons has not been investigated. We classified nestin-positive cells based on the length of their processes. Nestin single-positive cells were predominantly long, whereas most UCH-L1/nestin double-positive cells were predominantly short (Fig. 5). These results suggest that UCH-L1 plays a role in regulating NPC process length. We examined this possibility by inducing UCH-L1 in nestin-positive cells. Untransfected, proliferating nestin-positive NPCs had mainly long and bipolar processes [Fig. 3A, bFGF (48 hours)], but when UCH-L1 was transfected, the length of nestin-positive NPC processes shortened (Fig. 6A). The unipolar population increased following UCH-L1 expression. These results support the idea that UCH-L1 regulates NPC morphology. This idea was further confirmed by observations in NPCs from *gad* mice; as shown in Fig. 7B, NPCs from homozygous *gad* mice had longer processes than those from heterozygous controls. In addition, we observed that transfection of UCH-L1 shortened the processes of NPCs from *gad* mice compared with mock transfectants (Fig. 7C).

Our results also suggest that at least two populations of NPCs exist in the embryonic brain. The populations can be classified by the presence or absence of UCH-L1. In the dentate gyrus of the adult mouse brain, there are two distinct subpopulations of nestin-positive cells (Fukuda et al., 2003): those having short processes differentiate into neurons, whereas those having long processes generate late progenitors, which have short processes. The nestin staining pattern of brains from *gad* mice differed from that of brains from heterozygous littermates (Fig. 1). In the *gad* mouse brain, nestin-positive radial fibers were prominent, and almost all progenitor cells appeared to have long processes (Fig. 1). Since UCH-L1 affected NPC morphology (Fig. 6A and Fig. 7C), the difference in vivo indicates that differentiation itself was modulated by the absence of UCH-L1. Considering that neurons are present in the *gad* mouse even though it lacks UCH-L1 expression, further investigation into the morphological role of UCH-L1 using various approaches including the BrdU studies should provide important information about the heterogeneity of cortical neurons.

UCHs hydrolyze ubiquitin C-terminal small adducts in vitro (Larsen et al., 1998). Recently, a significant relationship was reported between UCH-L1 hydrolase activity and cell proliferation in lung cancer cell lines (Liu et al., 2003). We previously demonstrated that UCH-L1 extends ubiquitin half-life and prevents ubiquitin degradation. This function depends on the interaction between UCH-L1 and monoubiquitin but not on hydrolase activity (Osaka et al., 2003). In the present study, WT UCH-L1 and the C90S mutant both decreased the length of NPC processes. Both molecules associate with monoubiquitin, unlike another mutant, D30A, which did not affect process length (Fig. 6). Similar results were obtained from the transfection study using nestin-positive NPCs from *gad* mice (Fig. 7C). Thus, the effect of UCH-L1 on NPC process length is dependent on the interaction between UCH-L1 and ubiquitin but not on hydrolase activity. Although we did not examine the ligase activity of each mutant (Liu et al., 2002), the C90S mutant is unlikely to have ligase activity, because conjugation of ubiquitin to the C90S mutant forms a stable complex that prevents the release of ubiquitin (Sullivan and Vierstra, 1993). This observation suggests that the ligase activity is not related to the morphological changes that occurred in NPCs.

The ubiquitin system has an essential role in various physiological events, including cell-cycle progression, specific gene transcription, membrane protein trafficking, reversal of stress damage and intracellular signaling (Weissman, 2001). In cortical neurogenesis, the role of the ubiquitin system is not well understood. Several molecules that are important in cortical neurogenesis, including Notch, P35 and Dab1, are ubiquitylated (Arnaud et al., 2003; Bock et al., 2004; Patrick et al., 1998; Qiu et al., 2000). Here we show for the first time that UCH-L1 is expressed in NPCs and regulates their morphology. In addition, in vivo UCH-L1 expression is localized to the VZ and cortical layers that are undergoing neurogenesis. Cells undergoing gliogenesis had little UCH-L1 expression in vivo. These results suggest that UCH-L1 facilitates neurogenesis, an activity that appears to depend on the affinity of UCH-L1 for ubiquitin.

Materials and Methods

Animals

Pregnant C57BL/6J mice were purchased from CLEA Japan. The *gad* mouse is an autosomal recessive mutant that was obtained by crossing CBA and RFM mice (Saigoh et al., 1999). The *gad* line was maintained by intercrossing for more than 20 generations (Kwon et al., 2003; Saigoh et al., 1999). All animal experiments were performed in the laboratory according to the NIH Standards for Treatment of Laboratory Animals.

Antibodies and reagents

Monoclonal and polyclonal antibodies used in this study were as follows: monoclonal anti-nestin antibody (Becton Dickinson; and Rat401, Developmental Studies Hybridoma Bank, The University of Iowa, Iowa City, IA), monoclonal anti-neuronal tubulin β III antibody (TuJ1; Covance), polyclonal anti-UCH-L1 antibody (PGP9.5; RA95101, UltraClone), and polyclonal anti-FLAG antibody (Sigma). All secondary polyclonal antibodies conjugated to Alexa Fluor fluorescein were purchased from Molecular Probes.

Cortical NPC culture and differentiation conditions in C57BL/6 mice

Cortical NPCs were cultured as previously described (Nakashima et al., 1999). Briefly, embryos were removed from pregnant C57BL/6J mice (CLEA Japan) and staged according to morphological criteria to confirm the gestational day (Kaufman et al., 1998). Developing mouse cerebral cortex was dissected from E14 embryos. Cells were mechanically dissociated by trituration and plated at a concentration of 3.0×10^6 cells per 10 cm dish (Becton Dickinson) precoated with 10 ml of 15 μg/ml poly-L-ornithine (Sigma) and 10 ml of 1 μg/ml fibronectin (Nitta Gelatin). Cells were expanded for 5 days in serum-free neurobasal (NB) medium (Invitrogen) supplemented with B27 (Invitrogen), 0.5 mM L-glutamine (Invitrogen), 100 U/ml penicillin and 100 μg/ml streptomycin (Invitrogen). This medium contained 10 ng/ml bFGF (PeproTech). Cultures were maintained at 37°C in an atmosphere of 95% air and 5% CO_2. For secondary culture, bFGF-expanded NPCs were washed in warm Hank's Balanced Salt Solution, detached with mechanical pipetting, and resuspended in NB medium supplemented with B27, but not bFGF. Cells were then replated in 24-well plates (Nunc; 1.8×10^5 cells per well) that were precoated with 500 μl of 15 μg/ml poly-L-ornithine and 500 μl of 1 μg/ml fibronectin for immunofluorescence staining at each time point.

Cortical NPC culture and differentiation conditions in *gad* mice

Culture of NPCs derived from *gad* mice was performed as with NPCs derived from B6 mice. Developing mouse cerebral cortex was dissected from embryos at E13.5 to E14.5. The precise gestational day was determined according to previously established morphological criteria (Kaufman et al., 1998). NPCs from each embryo were collected and cultured separately. Each genotype was determined later using PCR and, as a result, each pair of *gad* and control littermate mice from two sets of

parents were used. Each culture of NPCs was replated in 24-well plates without bFGF and stained using anti-UCH-L1 24 hours after plating.

Immunohistochemistry

Brain sections were stained as previously described (Li et al., 2003; Osaka et al., 2003). Briefly, E14 and E16 mouse brains were removed and fixed in 4% paraformaldehyde/phosphate-buffered saline (PBS) for 2 hours at room temperature, cryoprotected in 30% sucrose in PBS and frozen in dry ice. Sections (20 μm thick) were cut on a cryostat, and mounted on aminopropylsilane (APS)-coated glass slides. They were then washed three times in PBS for 5 minutes, and blocked for 1 hour at room temperature with 3% bovine serum albumin, 2% (v/v) normal goat serum, and 0.2% (v/v) Triton X-100 in PBS (pH 7.4). Sections were incubated with primary antibodies [anti-nestin antibody (Rat401) 1:10; or anti-UCH-L1 antibody (RA95101) 1:4000; or anti-TuJ1 antibody, 1:1000] overnight at 4°C or for 2 hours at room temperature. After rinsing in PBS, the sections were incubated for 2 hours with diluted fluorescein-conjugated secondary antibody (1:200). The images were obtained with a confocal laser scanning TCS SL microscope, and detailed analyses were performed using an LSC confocal microscope system (Leica). Immunofluorescence intensities were measured from confocal images with Mac SCOPE software (version 2.59; Mitani).

Immunocytochemistry

Cells were stained as previously described (Aoki et al., 2002). Briefly, all incubations and washes were performed at room temperature. Cells were fixed with 3.8% formaldehyde/PBS for 10 minutes and permeabilized with 0.02% (v/v) Triton X-100/PBS for 5 minutes. Fixed cells were blocked with 3.3% goat serum for 30 minutes. Cells were incubated with a diluted primary polyclonal or monoclonal antibody (both were used for double staining) for 0.5-1 hour. The cells were then incubated with diluted secondary antibody conjugated to fluorescein for 0.5-1 hour. Antibody dilutions were as follows: anti-UCH-L1 antibody, 1:4000; anti-nestin antibody, 1:500; anti-TuJ1, 1:500. All secondary antibodies were diluted 1:200 in 1% goat serum/PBS before use. The images were obtained with fluorescence microscopy on an IX70 microscope (Olympus).

Transfection

For C57BL/6 mice, cells replated in 24-well plates were cultured overnight in growth medium containing bFGF and B27. The next day, each construct was transfected using Lipofectamine 2000 (Invitrogen) according to the manufacturer's instructions. NPCs were allowed to proliferate for 48 hours after transfection and then induced to differentiate for 12 hours without bFGF. For *gad*-mouse-derived NPCs, transfection was done in a similar manner.

Expression plasmids for human UCH-L1 variants

Mutant cDNAs encoding human UCH-L1 containing either the D30A or C90S substitution were obtained using the QuikChange site-directed mutagenesis kit (Stratagene) with the following mutagenesis oligonucleotides: 5′-CAGTGG-CGCTTCGTGGCCGTGCTGGGGCTGGAAG-3′ and 5′-CTTCCAGCCCCAG-CACGGCCACGAAGCGCCACTG-3′ for D30A; 5′-CCATTGGGAATTCCTCT-GGCACAATCGGAC-3′ and 5′-GTCCGATTGTGCCACAGGAATTCCCAA-TGG-3′ for C90S. Each single-nucleotide mutation in the resulting plasmids was confirmed by sequencing. Mammalian expression plasmids containing either FLAG-tagged human WT UCH-L1 or the D30A or C90S mutants were constructed using a pCI-*neo* mammalian expression vector (Promega). Bacterial expression plasmids containing either 6HN-tagged human WT UCH-L1 or the D30A or C90S mutants were constructed using a tetracycline-inducible expression system. *Xho*I-*Not*I cDNA fragments of the pCI-*neo* WT UCH-L1 or the D30A and C90S mutants and constructs were digested, and the DNA fragments were ligated between the *Sal*I and *Not*I sites in pPROtetE233 (Clontech) to generate pPROtetE233 6HN-tagged human WT, D30A and C90S UCH-L1 vectors. These expression plasmids were confirmed by sequencing.

In vitro assay for human UCH-L1 activity

Purified human UCH-L1 and the fluorogenic substrate ubiquitin-7-amino-4-methylcoumarin (Ub-AMC; Boston Biochem) were used to determine steady-state kinetic parameters as described previously (Nishikawa et al., 2003).

Immunoprecipitation

NIH-3T3 cells stably expressing human WT UCH-L1 or the C90S or D30A mutants, all with an HA-FLAG double tag at the N terminus, were cultured to subconfluency in a 10 cm dish, lyzed with 1 ml of modified RIPA buffer [50 mM Tris-HCl, pH 7.5, 1% (v/v) NP-40, 0.25% sodium deoxycholate, 150 mM NaCl, 1 mM EDTA] with EDTA-free complete protease inhibitor cocktail (Roche), sonicated and centrifuged at 18,000 *g* for 20 minutes at 4°C. Immunoprecipitation was performed as described previously (Ogawa et al., 2002).

Statistics

Statistical analyses were performed using StatView, version 5.0 (SAS) and Prism, version 3 (GraphPad Software). Analysis of variance (ANOVA) was used to assess differences between groups. A P value of less than 0.05 was considered statistically significant. When ANOVA results were statistically significant, they were examined by Fisher's PLSD, or Dunnett's multiple comparison test, or Bonferroni-Dunn multiple comparisons post hoc test. Differences between *gad* mice and control mice were analyzed using the Mann-Whitney U test.

The authors thank Yuh Nung Jan and Hua-Shun Li for providing the immunohistochemistry methods; Yoshihiro Nakatani and Hidesato Ogawa for providing the retroviral expression system and immunoprecipitation methods; and Masako Shikama for the care and breeding of animals. This work was supported by Grants-in-Aid for Scientific Research from the Ministry of Health, Labour and Welfare of Japan, and Grants-in-Aid for Scientific Research from the Ministry of Education, Culture, Sports, Science and Technology of Japan.

References

Aoki, S., Su, Q., Li, H., Nishikawa, K., Ayukawa, K., Hara, Y., Namikawa, K., Kiryu-Seo, S., Kiyama, H. and Wada, K. (2002). Identification of an axotomy-induced glycosylated protein, AIGP1, possibly involved in cell death triggered by endoplasmic reticulum-Golgi stress. *J. Neurosci.* **22**, 10751-10760.

Arnaud, L., Ballif, B. A. and Cooper, J. A. (2003). Regulation of protein tyrosine kinase signaling by substrate degradation during brain development. *Mol. Cell. Biol.* **23**, 9293-9302.

Bock, H. H., Jossin, Y., May, P., Bergner, O. and Herz, J. (2004). Apolipoprotein E receptors are required for reelin-induced proteasomal degradation of the neuronal adaptor protein Disabled-1. *J. Biol. Chem.* **279**, 33471-33479.

Dickson, D. W., Schmidt, M. L., Lee, V. M., Zhao, M. L., Yen, S. H. and Trojanowski, J. Q. (1994). Immunoreactivity profile of hippocampal CA2/3 neurites in diffuse Lewy body disease. *Acta Neuropathol. (Berl.)* **87**, 269-276.

Fukuda, S., Kato, F., Tozuka, Y., Yamaguchi, M., Miyamoto, Y. and Hisatsune, T. (2003). Two distinct subpopulations of nestin-positive cells in adult mouse dentate gyrus. *J. Neurosci.* **23**, 9357-9366.

Hartfuss, E., Forster, E., Bock, H. H., Hack, M. A., Leprince, P., Luque, J. M., Herz, J., Frotscher, M. and Gotz, M. (2003). Reelin signaling directly affects radial glia morphology and biochemical maturation. *Development* **130**, 4597-4609.

Hashimoto, M. and Mikoshiba, K. (2004). Neuronal birthdate-specific gene transfer with adenoviral vectors. *J. Neurosci.* **24**, 286-296.

Kaufman, M. H., Brune, R. M., Davidson, D. R. and Baldock, R. A. (1998). Computer-generated three-dimensional reconstructions of serially sectioned mouse embryos. *J. Anat.* **193**, 323-336.

Kawauchi, T., Chihama, K., Nabeshima, Y. and Hoshino, M. (2003). The in vivo roles of STEF/Tiam1, Rac1 and JNK in cortical neuronal migration. *EMBO J.* **22**, 4190-4201.

Kwon, J., Kikuchi, T., Setsuie, R., Ishii, Y., Kyuwa, S. and Yoshikawa, Y. (2003). Characterization of the testis in congenitally ubiquitin carboxy-terminal hydrolase-1 (Uch-L1) defective (gad) mice. *Exp. Anim.* **52**, 1-9.

Larsen, C. N., Krantz, B. A. and Wilkinson, K. D. (1998). Substrate specificity of deubiquitinating enzymes: ubiquitin C-terminal hydrolases. *Biochemistry* **37**, 3358-3368.

Leroy, E., Boyer, R., Auburger, G., Leube, B., Ulm, G., Mezey, E., Harta, G., Brownstein, M. J., Jonnalagada, S., Chernova, T. et al. (1998). The ubiquitin pathway in Parkinson's disease. *Nature* **395**, 451-452.

Li, H. S., Wang, D., Shen, Q., Schonemann, M. D., Gorski, J. A., Jones, K. R., Temple, S., Jan, L. Y. and Jan, Y. N. (2003). Inactivation of Numb and Numblike in embryonic dorsal forebrain impairs neurogenesis and disrupts cortical morphogenesis. *Neuron* **40**, 1105-1118.

Liu, Y., Fallon, L., Lashuel, H. A., Liu, Z. and Lansbury, P. T., Jr (2002). The UCH-L1 gene encodes two opposing enzymatic activities that affect alpha-synuclein degradation and Parkinson's disease susceptibility. *Cell* **111**, 209-218.

Liu, Y., Lashuel, H. A., Choi, S., Xing, X., Case, A., Ni, J., Yeh, L. A., Cuny, G. D., Stein, R. L. and Lansbury, P. T., Jr (2003). Discovery of inhibitors that elucidate the role of UCH-L1 activity in the H1299 lung cancer cell line. *Chem. Biol.* **10**, 837-846.

Malatesta, P., Hartfuss, E. and Gotz, M. (2000). Isolation of radial glial cells by fluorescent-activated cell sorting reveals a neuronal lineage. *Development* **127**, 5253-5263.

Malatesta, P., Hack, M. A., Hartfuss, E., Kettenmann, H., Klinkert, W., Kirchhoff, F. and Gotz, M. (2003). Neuronal or glial progeny: regional differences in radial glia fate. *Neuron* **37**, 751-764.

McQuaid, S., McConnell, R., McMahon, J. and Herron, B. (1995). Microwave antigen retrieval for immunocytochemistry on formalin-fixed, paraffin-embedded post-mortem CNS tissue. *J. Pathol.* **176**, 207-216.

Nadarajah, B., Brunstrom, J. E., Grutzendler, J., Wong, R. O. and Pearlman, A. L. (2001). Two modes of radial migration in early development of the cerebral cortex. *Nat. Neurosci.* **4**, 143-150.

Nakashima, K., Yanagisawa, M., Arakawa, H., Kimura, N., Hisatsune, T., Kawabata, M., Miyazono, K. and Taga, T. (1999). Synergistic signaling in fetal brain by STAT3-Smad1 complex bridged by p300. *Science* **284**, 479-482.

Nishikawa, K., Li, H., Kawamura, R., Osaka, H., Wang, Y. L., Hara, Y., Hirokawa, T., Manago, Y., Amano, T., Noda, M. et al. (2003). Alterations of structure and

hydrolase activity of parkinsonism-associated human ubiquitin carboxyl-terminal hydrolase L1 variants. *Biochem. Biophys. Res. Commun.* **304**, 176-183.

Noctor, S. C., Flint, A. C., Weissman, T. A., Dammerman, R. S. and Kriegstein, A. R. (2001). Neurons derived from radial glial cells establish radial units in neocortex. *Nature* **409**, 714-720.

Noctor, S. C., Flint, A. C., Weissman, T. A., Wong, W. S., Clinton, B. K. and Kriegstein, A. R. (2002). Dividing precursor cells of the embryonic cortical ventricular zone have morphological and molecular characteristics of radial glia. *J. Neurosci.* **22**, 3161-3173.

Noctor, S. C., Martinez-Cerdeno, V., Ivic, L. and Kriegstein, A. R. (2004). Cortical neurons arise in symmetric and asymmetric division zones and migrate through specific phases. *Nat. Neurosci.* **7**, 136-144.

Ogawa, H., Ishiguro, K., Gaubatz, S., Livingston, D. M. and Nakatani, Y. (2002). A complex with chromatin modifiers that occupies E2F- and Myc-responsive genes in G0 cells. *Science* **296**, 1132-1136.

Osaka, H., Wang, Y. L., Takada, K., Takizawa, S., Setsuie, R., Li, H., Sato, Y., Nishikawa, K., Sun, Y. J., Sakurai, M. et al. (2003). Ubiquitin carboxy-terminal hydrolase L1 binds to and stabilizes monoubiquitin in neuron. *Hum. Mol. Genet.* **12**, 1945-1958.

Patrick, G. N., Zhou, P., Kwon, Y. T., Howley, P. M. and Tsai, L. H. (1998). p35, the neuronal-specific activator of cyclin-dependent kinase 5 (Cdk5) is degraded by the ubiquitin-proteasome pathway. *J. Biol. Chem.* **273**, 24057-24064.

Qian, X., Goderie, S. K., Shen, Q., Stern, J. H. and Temple, S. (1998). Intrinsic programs of patterned cell lineages in isolated vertebrate CNS ventricular zone cells. *Development* **125**, 3143-3152.

Qian, X., Shen, Q., Goderie, S. K., He, W., Capela, A., Davis, A. A. and Temple, S. (2000). Timing of CNS cell generation: a programmed sequence of neuron and glial cell production from isolated murine cortical stem cells. *Neuron* **28**, 69-80.

Qiu, L., Joazeiro, C., Fang, N., Wang, H. Y., Elly, C., Altman, Y., Fang, D., Hunter, T. and Liu, Y. C. (2000). Recognition and ubiquitination of Notch by Itch, a hect-type E3 ubiquitin ligase. *J. Biol. Chem.* **275**, 35734-35737.

Rice, D. S. and Curran, T. (2001). Role of the reelin signaling pathway in central nervous system development. *Annu. Rev. Neurosci.* **24**, 1005-1039.

Roegiers, F. and Jan, Y. N. (2004). Asymmetric cell division. *Curr. Opin. Cell Biol.* **16**, 195-205.

Saigoh, K., Wang, Y. L., Suh, J. G., Yamanishi, T., Sakai, Y., Kiyosawa, H., Harada, T., Ichihara, N., Wakana, S., Kikuchi, T. et al. (1999). Intragenic deletion in the gene encoding ubiquitin carboxy-terminal hydrolase in gad mice. *Nat. Genet.* **23**, 47-51.

Satoh, J. and Kuroda, Y. (2001). A polymorphic variation of serine to tyrosine at codon 18 in the ubiquitin C-terminal hydrolase-L1 gene is associated with a reduced risk of sporadic Parkinson's disease in a Japanese population. *J. Neurol. Sci.* **189**, 113-117.

Sauvageot, C. M. and Stiles, C. D. (2002). Molecular mechanisms controlling cortical gliogenesis. *Curr. Opin. Neurobiol.* **12**, 244-249.

Schofield, J. N., Day, I. N., Thompson, R. J. and Edwards, Y. H. (1995). PGP9.5, a ubiquitin C-terminal hydrolase; pattern of mRNA and protein expression during neural development in the mouse. *Brain Res. Dev. Brain Res.* **85**, 229-238.

Sekiguchi, S., Yoshikawa, Y., Tanaka, S., Kwon, J., Ishii, Y., Kyuwa, S., Wada, K., Nakamura, S. and Takahashi, K. (2003). Immunohistochemical analysis of protein gene product 9.5, a ubiquitin carboxyl-terminal hydrolase, during placental and embryonic development in the mouse. *Exp. Anim.* **52**, 365-369.

Shen, Q., Qian, X., Capela, A. and Temple, S. (1998). Stem cells in the embryonic cerebral cortex: their role in histogenesis and patterning. *J. Neurobiol.* **36**, 162-174.

Sullivan, M. L. and Vierstra, R. D. (1993). Formation of a stable adduct between ubiquitin and the Arabidopsis ubiquitin-conjugating enzyme, AtUBC1+. *J. Biol. Chem.* **268**, 8777-8780.

Tabata, H. and Nakajima, K. (2003). Multipolar migration: the third mode of radial neuronal migration in the developing cerebral cortex. *J. Neurosci.* **23**, 9996-10001.

Temple, S. (2001). The development of neural stem cells. *Nature* **414**, 112-117.

Weissman, A. M. (2001). Themes and variations on ubiquitylation. *Nat. Rev. Mol. Cell. Biol.* **2**, 169-178.

Wilkinson, K. D., Lee, K. M., Deshpande, S., Duerksen-Hughes, P., Boss, J. M. and Pohl, J. (1989). The neuron-specific protein PGP 9.5 is a ubiquitin carboxyl-terminal hydrolase. *Science* **246**, 670-673.

Zhong, W., Feder, J. N., Jiang, M. M., Jan, L. Y. and Jan, Y. N. (1996). Asymmetric localization of a mammalian numb homolog during mouse cortical neurogenesis. *Neuron* **17**, 43-53.

Zhong, W., Jiang, M. M., Weinmaster, G., Jan, L. Y. and Jan, Y. N. (1997). Differential expression of mammalian Numb, Numblike and Notch1 suggests distinct roles during mouse cortical neurogenesis. *Development* **124**, 1887-1897.

BRAIN RESEARCH 1070 (2006) 1-14

available at www.sciencedirect.com

SCIENCE DIRECT

www.elsevier.com/locate/brainres

BRAIN RESEARCH

Research Report

Identification and functional characterization of mouse TPO1 as a myelin membrane protein

Nobuna Fukazawa[a,c,1], *Koichi Ayukawa*[a,1], *Kaori Nishikawa*[a], *Hiroki Ohashi*[a,f], *Nobutsune Ichihara*[d], *Yuki Hikawa*[a], *Toshiaki Abe*[f], *Yoshihisa Kudo*[c], *Hiroshi Kiyama*[e], *Keiji Wada*[a], *Shunsuke Aoki*[a,b,*]

[a]*Department of Degenerative Neurological Diseases, National Institute of Neuroscience, National Center of Neurology and Psychiatry, Kodaira, Tokyo 187-8502, Japan*

[b]*Department of Demyelinating Disease and Aging, National Institute of Neuroscience, National Center of Neurology and Psychiatry, Kodaira, Tokyo 187-8502, Japan*

[c]*Laboratory of Cellular Neurobiology, Tokyo University of Pharmacology and Life Science, Hachioji, Tokyo 192-0392, Japan*

[d]*Department of Anatomy, School of Veterinary Medicine, Azabu University, Sagamihara 229-8501, Japan*

[e]*Department of Anatomy, Graduate School of Medicine, Osaka City University, Asahimachi, Abenoku, Osaka 545-8585, Japan*

[f]*Department of Neurosurgery, Jikei University School of Medicine, Minatoku, Tokyo 105-8401, Japan*

ARTICLE INFO

Article history:
Accepted 17 November 2005
Available online 6 January 2006

Keywords:
Myelin
Oligodendrocyte
Schwann cell
Fyn
AIGP

ABSTRACT

TPO1 is a member of the AIGP family, a unique group of proteins that contains 11 putative transmembrane domains. Expression of the rat TPO1 gene is upregulated in cultured oligodendrocytes (OLs) during development from pro-oligodendroblasts to postmitotic OLs. However, the distribution of native TPO1 protein in cultured OLs and in the brain has not been elucidated. We investigated the distribution and cellular function of TPO1 in myelinating cells of the nervous system. In mice, TPO1 gene expression was detected in the central (CNS) and peripheral (PNS) nervous systems and was markedly upregulated at postnatal days 10–20, an early phase of myelination in the mouse brain. To investigate TPO1 localization, we generated affinity-purified antibodies to synthetic peptides derived from mouse TPO1. Immunohistochemical analysis showed that TPO1 was expressed in OLs and Schwann cells but not in neurons and astrocytes. Schwann cells from trembler mice, which lack PNS myelin, had significantly decreased TPO1 expression and an altered localization pattern, suggesting that TPO1 is a functional myelin membrane protein. In OL lineage cell cultures, TPO1 was detected in A2B5(+) bipolar early progenitors, A2B5(+) multipolar Pro-OLs, GalC(+) immature OLs and MBP(+) mature OLs. The subcellular localization of TPO1 in OL lineage cells was mapped to the GM130(+) Golgi in cell bodies and Fyn(+) cell processes and myelin-like sheets. Furthermore, TPO1 selectively colocalized with non-phosphorylated Fyn and promoted Fyn autophosphorylation in COS7 cells, suggesting that TPO1 may play a role in myelin formation via Fyn kinase activation in the PNS and CNS.

* *Corresponding author.* Department of Degenerative Neurological Diseases, National Institute of Neuroscience, National Center of Neurology and Psychiatry, 4-1-1, Ogawahigashi, Kodaira, Tokyo 187-8502, Japan. Fax: +81 42 346 1745.
E-mail address: aokis@ncnp.go.jp (S. Aoki).

[1] These two authors contributed equally to this work.

0006-8993/$ – see front matter © 2005 Elsevier B.V. All rights reserved.
doi:10.1016/j.brainres.2005.11.069

Abbreviations:
aa, amino acid
AIGP, axotomy-induced glycosylated/Golgi-complex protein
CNS, central nervous system
DMEM, Dulbecco's modified Eagle' medium
EEA1, early endosome antigen1
EGFP, enhanced green fluorescent protein
ER, endoplasmic reticulum
GalC, galactocerebroside
GAPDH, glyceraldehyde-3-phosphate dehydrogenase
GFAP, glial fibrillary acidic protein
HRP, horseradish peroxidase
Lamp-1, lysosome-associated membrane glycoprotein-1
MAG, myelin-associated glycoprotein
Map-2, microtubule-associated protein-2
MBP, myelin basic protein
nt, nucleotide
MOG, myelin oligodendrocyte glycoprotein
MyTI, myelin transcriptional factor I
OL, oligodendrocyte
OPC, oligodendrocyte precursor cell
ORF, open reading frame
P0, myelin protein zero
PBS, phosphate-buffered saline
PLP, proteolipid protein
PMP22, peripheral myelin protein-22
PNS, peripheral nervous system
T-TBS, Tris-buffered saline containing 0.1% (v/v) Tween-20

1. Introduction

Schwann cells and oligodendrocytes (OLs) produce myelin in the PNS and CNS, respectively. Myelin is composed of lamellar membranes and ensheaths axons and is essential for nervous system function, as demonstrated by the severe neurological symptoms observed in various myelin diseases (Baumann and Pham-Dinh, 2001; Shy et al., 2002). A number of myelin membrane proteins have been identified to date and have been shown to play pivotal roles in myelin construction and maintenance (Baumann and Pham-Dinh, 2001). Myelin-associated glycoprotein (MAG) is a single transmembrane protein and has multiple immunoglobulin domains, and MAG-deficient mice show delayed myelin compaction (Li et al., 1994). Myelin OL glycoprotein (MOG) is a CNS myelin-specific, single-transmembrane protein that induces experimental autoimmune encephalomyelitis (Scolding et al., 1989; Weissert et al., 1998). Proteolipid protein (PLP) is the most abundant myelin membrane protein, comprising 50% of total myelin protein, and is a member of the tetraspan protein family. Studies in jumpy mice and human Pelizaeus–Merzbacher disease have shown that PLP is essential for stabilizing the myelin membrane (Klugmann et al., 1997; Baumann and Pham-Dinh, 2001). Peripheral myelin protein-22 (PMP22), another member of the tetraspan protein family, and myelin protein zero (P0), a single-transmembrane domain protein, specifically localize to PNS myelin membranes, and the genes encoding these proteins are among those causing Charcot–Marie–Tooth disease (Sakamoto et al., 1987; Lupski et al., 1991; Suter et al., 1992; Suh et al., 1997; Sakai et al., 1999).

AIGP1 (axotomy-induced glycosylated/Golgi complex protein 1) is a neuronal membrane protein that specifically localizes to Golgi membranes in neurons. AIGP1 has eleven potential transmembrane helices. Previously, we reported the possible involvement of AIGP1 in axotomy-associated neuronal cell death (Aoki et al., 2002). The AIGP family genes are evolutionarily conserved from yeast to mammals and, in mammals, consist of three members AIGP1, TMS-2 (Grossman et al., 2000; Aoki et al., 2002) and TPO1 (Krueger et al., 1997). The rat TPO1 gene was originally identified by

differential gene screening, and its expression was shown to be upregulated during OL differentiation (Krueger et al., 1997). Pfeiffer and coworkers also showed that the TPO1 gene is expressed in cultured OLs and rat brain (Krueger et al., 1997). However, the lack of availability of TPO1-specific antibodies has precluded elucidation of the natural distribution and function of this protein. Similarly to other proteins in the AIGP family, TPO1 is also a putative eleven-span membrane protein. However, the putative TPO1 amino acid sequence also has features that distinguish it from other AIGP family members; these features include an extremely polarized structure (N-terminal basic and C-terminal acidic composition), a sequence homologous to myelin transcriptional factor I (MyTI) and a potential C-terminal palmitoylation sequence (Krueger et al., 1997). Accordingly, the cell type-specific expression patterns of TPO1 are distinct from those of the AIGP1 and TMS-2 genes in the nervous system; AIGP1 and TMS-2 are specifically expressed in neurons (Grossman et al., 2000; Aoki et al., 2002), whereas the rat TPO1 gene is expressed in OL lineage cells (Krueger et al., 1997). AIGP1 has been suggested to function as a cell death regulator in axotomized neurons (Aoki et al., 2002), but the biological function of TPO1 is not known.

In this study, we used TPO1-specific antibodies to investigate the localization of TPO1 and to characterize its function in the nervous system. We show that TPO1 is a myelin membrane protein that possibly promotes autophosphorylation of Fyn kinase. Our results suggest that TPO1, a glial subtype of the AIGP family, may play a role in myelin formation and maintenance by regulating Fyn kinase activity.

2. Results

2.1. *Identification of mouse TPO1*

While screening for molecules involved in neuronal regeneration and death, we previously identified a mouse axotomy-induced glycosylated/Golgi complex protein, AIGP1 (Grossman et al., 2000; Aoki et al., 2002). Database searches suggested that the mouse or rat genome encodes three AIGP1 homologs: AIGP1, TMS-2 (GenBank accession no. AF181685) and TPO1 (GenBank accession no. L20319) (Fig. 1A). In mice, the AIGP1 and TMS-2 genes are expressed in neurons in the cortex, hippocampus, cerebellum and hypoglossal nucleus (Grossman et al., 2000; Aoki et al., 2002). On the other hand, in rats, the TPO1 gene has been reported to be expressed in OL lineage cells in vitro (Krueger et al., 1997). Since the cell type-specific expression pattern of TPO1 suggests distinct functionality, we were interested in the molecular function of TPO1 in the nervous system. The mouse TPO1 cDNA sequence (GenBank accession no. AB029501, (Aoki et al., 2002)) contains a 1416-bp open reading frame (ORF) that is homologous to the rat TPO1 cDNA sequence (57.7%). The ORF encodes 462 aa with 90% similarity to rat TPO1. Mouse AIGP1 and TMS-2 are less similar (36.8% and 39%, respectively) to mouse TPO1 (data not shown). The sequence of TPO1 is less conserved compared with AIGP1 and TMS-2 (Grossman et al., 2000; Aoki et al., 2002). Computational analyses with the transmembrane prediction software SOSUI (http://sosui.proteome.bio.tuat.ac.jp) suggest that TPO1 has eleven putative transmembrane helices (Fig. 1B). The second and fourth extracellular loops and fifth intracellular loop have relatively longer structures than the other loops (Fig. 1B), but the amino acid sequences of the long loops are not well conserved between TPO1 and other family members (data not shown). Two cysteine-rich zinc finger-like motifs, $CX_5CX_{6-10}CX_2C$ (residues 6–27, similar to aminoacyl tRNA synthetases) and $CX_5CX_1CX_4H$ (residues 100–123, similar to transcription factor MYT1; (Hirayama et al., 2003), and a potential C-terminal palmitoylation sequence (residues 453–454) were also found in the TPO1 sequence (Fig. 1B, Krueger et al., 1997). These motifs are highly conserved between rats and mice, but are not present in mouse AIGP1 and TMS-2 (data not shown). Two potential N-linked glycosylation sites (Asn-X-Thr) were identified in both AIGP1 and TMS-2 (Grossman et al., 2000; Aoki et al., 2002), but such sites were not found in the amino acid sequence of TPO1 (data not shown). Two potential phosphorylation sites for protein kinase C were identified in the second and third intracellular loops, and one potential target site for cAMP-dependent protein kinase was found in the fifth intracellular loop of TPO1 (data not shown). Phylogenetic analysis of the AIGP family members showed that mouse and rat TPO1 form a cluster that is completely separate from the AIGP1 and TMS-2 clusters (Fig. 1A).

2.2. *TPO1 expression in the PNS and CNS*

Previous studies (Krueger et al., 1997) have shown that the rat TPO1 gene is expressed in the CNS and in OL lineage cells. To examine gene expression levels in the PNS and CNS precisely, we performed SYBR green-based real-time RT-PCR analysis with the mouse CNS and PNS myelin-specific markers MOG (Scolding et al., 1989) and P0 (Sakamoto et al., 1987; Lupski et al., 1991) (Fig. 1C, top). We examined TPO1 gene expression in the mouse dorsal root ganglion and brain. Both PNS and CNS tissues expressed TPO1 mRNA at considerable levels, which were remarkably higher than expression levels observed in the E14 brain (Fig. 1C, top). In the postnatal CNS, TPO1 gene expression markedly increased after P10 and reached a maximum level at P20. This level of expression was maintained throughout adult life (Fig. 1C, bottom).

2.3. *Production and characterization of antibodies to mouse TPO1*

We prepared specific antibodies against relatively hydrophilic peptide sequences of the fifth intracellular and second extracellular loops of mouse TPO1 (EP05 and EP06, respectively, [EP; epitope], Fig. 1B). Immunoblot analysis using mouse cultured OL cell lysates showed that anti-TPO1 (ABEP05; against EP05) recognized a ~48-kDa band (Fig. 2A, lane 2) that was slightly smaller than the expected molecular mass (51.8 kDa), probably because of its hydrophobicity (Fig. 2A, lane 2). No signal was detected when the blot was probed with control rabbit IgG (Fig. 2A, lanes 3 and 4). TPO1 was detected in the membrane fraction but not in the soluble fraction (Fig. 2A, lanes 1 and 2).

2.4. *Localization of TPO1 in the mouse PNS and CNS tissues*

To determine the localization of mouse TPO1 in the PNS and CNS, immunohistochemical analyses were performed with the TPO1-specific antibody, ABEP05. Mouse sciatic nerves and cerebellar medulla both showed myelin-like immunoreactivity (Figs. 2B, b–d), whereas staining with negative control rabbit IgG at the same concentration yielded no signal (Figs. 2B, a). TPO1 specifically localized to the OL-enriched regions in the CNS, including white matter tracts in the cerebrum, caudate–putamen (Figs. 2C, b and c) and cerebellum (Figs. 2C, e and f). Pre-absorption of ABEP05 with the epitope peptide EP05 abrogated the cerebrum signals (Figs. 2C, a), indicating that anti-TPO1 specifically recognized mouse TPO1 in vivo.

To determine the cell type-specific expression of TPO1 in the nervous system, we double-stained brain sections of adult mouse with anti-TPO1 and cell type-specific marker antibodies, including anti-MBP as a marker of both Schwann cells and OLs, anti-Map-2 as a neuron marker, and anti-GFAP as an astrocyte marker. TPO1 staining colocalized with MBP staining in the sciatic nerve (Figs. 3A a–c), white matter tracts of the cerebrum (Figs. 3B, a–c) and cerebellum (Figs. 3B d–f), but the staining did not overlap with that of Map-2 (Figs. 3C, a–c) or GFAP (Figs. 3C, d–f). In the cerebellum, TPO1 staining also overlapped with O4 staining (Figs. 3C, g–i). These data suggest that TPO1 localizes specifically to Schwann cells and OLs in the PNS and CNS, respectively.

2.5. *Mislocalized and decreased expression of mouse TPO1 in the PNS myelin membrane of the trembler-Ncnp mouse*

To confirm the specific expression of TPO1 in myelin-producing cells and to address whether it specifically

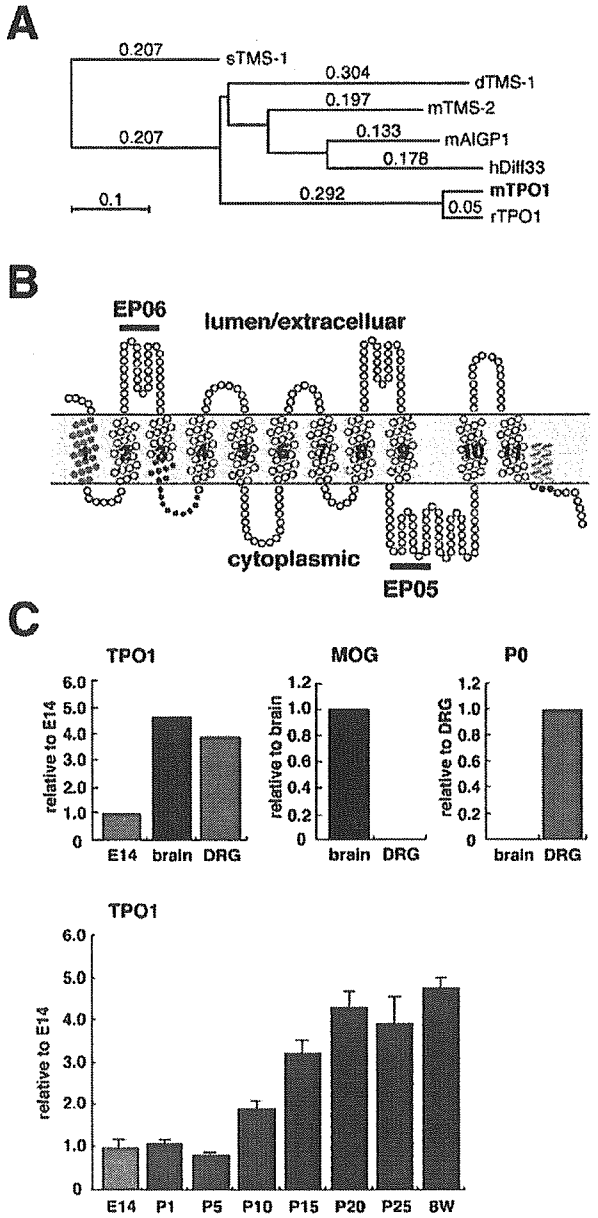

localizes to the myelin membrane in vivo, we examined the expression pattern of TPO1 in the sciatic nerve of adult trembler-Ncnp mice, which exhibit specific loss of MBP-positive myelin membranes in Schwann cells (Suh et al., 1997; Sakai et al., 1999). MBP staining was completely absent from the myelin in the sciatic nerve of trembler-Ncnp mice (Figs. 4A, e), indicating the loss of myelin membrane, whereas intact MBP-positive myelin membrane was detectable in wild-type mice (Figs. 4A, b). TPO1 staining was markedly decreased in trembler-Ncnp mice compared with wild-type mice (Figs. 4A, a and d; B, a and b), and small puncta of TPO1 staining remained in Schwann cells (Figs. 4B, b; arrowheads). These results clearly indicate that TPO1 is a myelin membrane protein in Schwann cells.

2.6. *Expression of TPO1 in OL lineage cells*

TPO1 staining colocalized with MBP staining in the PNS and CNS (Fig. 3), suggesting its specific localization in OLs and Schwann cells. Moreover, the loss of TPO1 staining in the sciatic nerve tissue of trembler-Ncnp mice indicated its specific localization to PNS myelin membranes (Fig. 4). However, gross immunostaining analyses of the CNS were not sufficient to confirm the localization of TPO1 in OLs. To test whether TPO1 is specifically expressed in OLs in the CNS, we performed immunostaining with anti-TPO1 in various types of cells isolated from the CNS, including mouse embryonic cortical neuroepithelial cells, rat optic nerve-derived OL lineage cells, mouse cortical neurons and astrocytes. TPO1 staining was not detectable in nestin (+) neuroepithelial cells (Figs. 5A, H and O). However, a small number of TPO1-expressing cells were detected in neuroepithelial cell cultures (Figs. 5A, H and O), and these cells are likely to be differentiated cells derived from neuroepithelial cells because of the absence of, or decrease in, nestin expression (Figs. 5A, H and O, arrowhead). The rat optic nerve-derived OL lineage cells, including A2B5(+) bipolar early progenitors (Figs. 5B, I and P), A2B5(+) multipolar Pro-OLs (Figs. 5C, J and Q), GalC(+) immature OLs (Figs. 5D, K and R) and MBP(+) mature OLs (Figs. 5E, L and S) all expressed TPO1. Map2(+) neurons and GFAP(+) astrocytes cultured in vitro showed no TPO1 staining (Figs. 5F, G, M, N, T, and U), in good agreement with the results of immunohistochemical analyses in intact tissues (Figs. 3C, a–f). Immunostaining with negative control IgG yielded no specific staining, and pre-adsorption of anti-TPO1 with antigen peptide abolished staining (data not shown).

2.7. *Subcellular localization of TPO1 in the Golgi and myelin in OLs*

To determine the subcellular localization of TPO1 in OLs, rat optic nerve-derived OLs were double labeled with organelle-specific markers, and confocal laser scan analyses were performed through all cell structures from the cell bodies (top) through cell processes and myelin-like sheets (bottom). TPO1 staining clearly overlapped with GM130 (Nakamura et al., 1995) staining in cell bodies (Figs. 6A, d, e and f), indicating localization to the Golgi complex in OL cell bodies. However, TPO1 staining did not overlap with that of other markers, including the endoplasmic reticulum marker KDEL (Vaux et al., 1990) (Figs. 6A, a, b and c) in cell bodies, and the lysosomal marker Lamp-1 (Chen et al., 1985) (Figs. 6B, a, b and c), the secretary vesicle marker Rab3a (Fukuda et al., 2002) (Figs. 6B, d, e and f) or the endosome marker EEA1 (Mu et al., 1995) (Figs. 6B, g, h and i) in cell processes and in myelin-like sheets.

TPO1 was expressed in OL lineage cells from early to terminal differentiation stages (Figs. 5B–E). We found that TPO1 staining overlapped with GalC staining in mature OLs (Figs. 6C a–c). The overlapping expression patterns suggested that TPO1 is a constituent of myelin membranes. TPO1 has cysteine residues at the C terminus, which is potentially palmitoylated (Krueger et al., 1997). Fyn tyrosine kinase (Fyn) has also been reported to be palmitoylated (Shenoy-Scaria et al., 1993; Koegl et al., 1994; Wolven et al., 1997) and is important for morphogenesis and myelin formation in OLs (Osterhout et al., 1999; Sperber and McMorris, 2001; Klein et al., 2002; Colognato et al., 2004; Liang et al., 2004). To determine the spatial relationship between TPO1 and Fyn, we double

Fig. 1 – Evolution, structure, and expression profile of mouse TPO1. (A) Phylogeny of amino acid sequences of AIGP family members. Multiple sequence alignment was generated using Clustal W software (Oxford Molecular Group plc, Oxford, UK), and the phylogenic tree was constructed from multiple sequence alignments using the neighbor-joining method with MacVector 7.0 (Oxford Molecular Group plc, Oxford, UK). The length of the horizontal lines indicates relative sequence divergence, and bootstrap probabilities are shown at each node. sTMS-1, *Saccharomyces cerevisiae* TMS-1 (Z47746); dTMS, *Drosophila melanogaster* TMS-1 (AF181686); mAIGP1, mouse AIGP1 (AB029499); mTMS-2, mouse TMS-2 (AF181685); hDiff33, human Diff33 (U49188); rTPO1, rat TPO1 (L20319). (B) Membrane topological model for TPO1. The model illustrates the predicted transmembrane domain and the extra- and intracellular loops. Each circle represents an amino acid, and transmembrane helices are numbered. Cysteine-rich motifs, $CX_5CX_{6-10}CX_2C$ (residues 6–27), are shown as red circles, and zinc-finger-like motifs, $CX_5CX_1CX_4H$ (residues 100–123), are shown in green. The potential C-terminal palmitoylation sequence (residues 453–454) is shown in cyan. EP05 (epitope 05) and EP06 (epitope 06) indicate the peptide antigens used for producing antibodies against mouse TPO1. (C) Gene expression profiles of mouse TPO1. Total RNA was isolated from whole heads of E14 mouse embryos, postnatal whole brains (P1–8 weeks) and dorsal root ganglia (DRG). Each cDNA was synthesized using an equal amount of total RNA. SYBR Green-based quantitative RT-PCR analysis of TPO1 transcripts in the mouse CNS and PNS was performed (top). The β-actin gene was used to normalize the intensities between samples and the MOG and P0 genes were used as controls for CNS- and PNS-specific genes, respectively. The relative gene expression levels from the mice brain and DRG are shown in comparison with the average expression level from E14 heads. The expression levels of TPO1 mRNA during mouse brain development are also shown (bottom). The relative gene expression levels of postnatal developing brains (P1–8 weeks) are shown in comparison with E14 heads. The β-actin gene was used as a calibrator. Each bar represents the mean ± SEM (n = 3; three heads or brains).

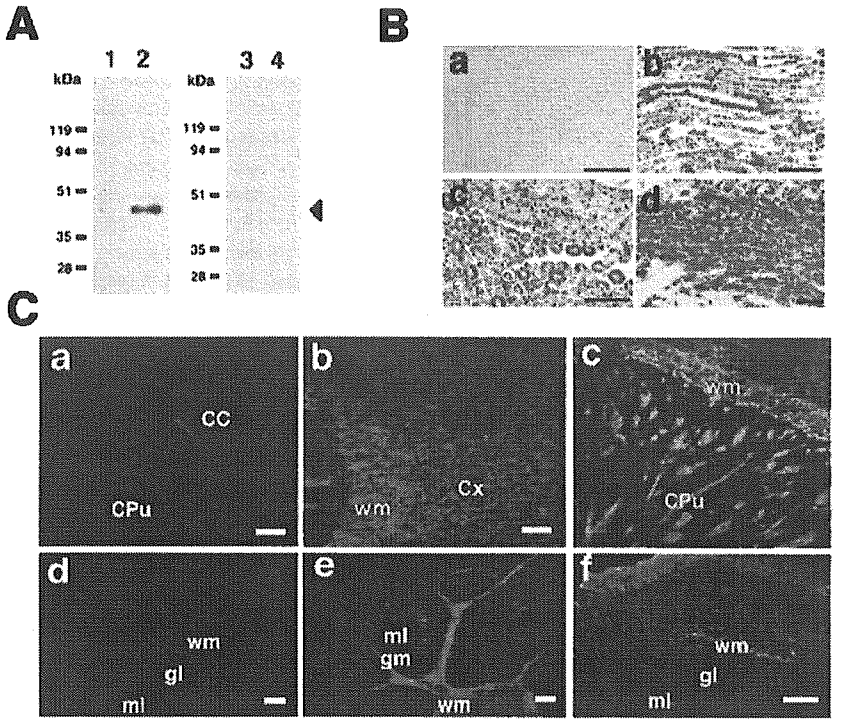

Fig. 2 – Localization of TPO1 in the PNS and CNS. (A) Immunoblot analysis of the soluble and insoluble fractions of OL-derived cell lysates using anti-TPO1 (ABEP05). OLs were lysed with detergent (–) buffer and separated into soluble and insoluble fractions. Soluble (lanes 1 and 3) and insoluble (lanes 2 and 4) fractions were subjected to SDS-PAGE and probed with anti-TPO1 (lanes 1 and 2) or normal rabbit IgG (lanes 3 and 4). The arrowhead indicates the apparent 48 kDa band corresponding to TPO1. (B) Immunohistochemical analyses of TPO1 in the PNS and CNS. Sections (paraffin; 5 μm thickness) were stained with anti-TPO1 (ABEP05; b–d) or normal rabbit IgG (a). Staining was visualized using the diaminobenzidine (DAB) method. Longitudinal (b) and transverse (c) sections of the sciatic nerve are shown. Staining of the cerebellar medulla is shown in d. Scale bars = 40 μm. (C) Localization of TPO1 in the mouse cerebrum (a–c) and cerebellum (d–f). Sagittal frozen sections (20 μm thickness) from P20 mouse brain were immunostained with anti-TPO1 (ABEP05; b, c, e and f). Staining with pre-absorbed antibody (epitope peptide 05; EP05) or normal rabbit IgG are shown in a and d, respectively. Images were obtained by confocal microscopy. CC, corpus callosum; Cx, cortex; CPu, caudate–putamen; ml, molecular cell layer; gl, granule cell layer; wm, white matter. Scale bars = 50 μm.

labeled OLs with antibodies against TPO1 and Fyn. TPO1 partially colocalized with Fyn in a punctate pattern within OL cell processes and myelin membranes (Figs. 6C d, e and f, and C 1 and 2, arrows).

2.8. *TPO1 predominantly colocalizes with non-phosphorylated Fyn tyrosine kinase, and may promote its phosphorylation*

To determine whether TPO1 is involved in the regulation of Fyn tyrosine kinase activity, the phosphorylation levels of Fyn and Src were analyzed in COS7 cells transfected with EGFP-TPO1 or EGFP expression constructs. Immunoblotting with anti-phospho-Src family protein antibodies (specifically recognizing both phospho-Tyr 420 of Fyn and phospho-Tyr 416 of Src) showed an elevated level (over twofold) of phosphorylated Fyn in COS7 cells transfected with EGFP-TPO1 compared with EGFP-transfected cells (Figs. 7I and K, left). The Src phosphorylation level was comparable between EGFP-TPO1- and EGFP-transfected cells (Figs. 7J and K, right). The amount of Fyn, Src and GAPDH (for internal control) protein was equivalent in all samples (Figs. 7I and J), indicating that the elevated level of phosphorylated Fyn was not due to a change in the amount of each protein per cell. While EGFP fluorescence in COS7 cells was uniformly distributed in the cytosol and nucleus, TPO1-EGFP localized to perinuclear Golgi complexes and pericellular puncta (Figs. 7C, D, G and H). In cells doubly transfected with Fyn and TPO1-EGFP constructs, the localization patterns of both proteins partially overlapped (Fig. 7G, arrowhead, and G′, arrows), but phosphorylated Fyn was completely segregated from TPO1 (Fig. 7H; arrowheads). This suggests that TPO1 predominantly colocalizes with non-phosphorylated Fyn and not with phosphorylated Fyn. Moreover, EGFP-TPO1-transfected cells showed increased staining for phosphorylated Fyn in pericellular regions (Fig. 7H; arrowheads) compared with EGFP-transfected cells (Fig. 7F), in good agreement with the results from immunoblot analyses (Figs. 7I and K, left). We failed to detect a complex containing TPO1 and Fyn using the immunoprecipitation assay; this was most likely a consequence of the fact that TPO1 is extremely hydrophobic and thus was not solubilized by detergents that is generally used in immunoprecipitation assays.

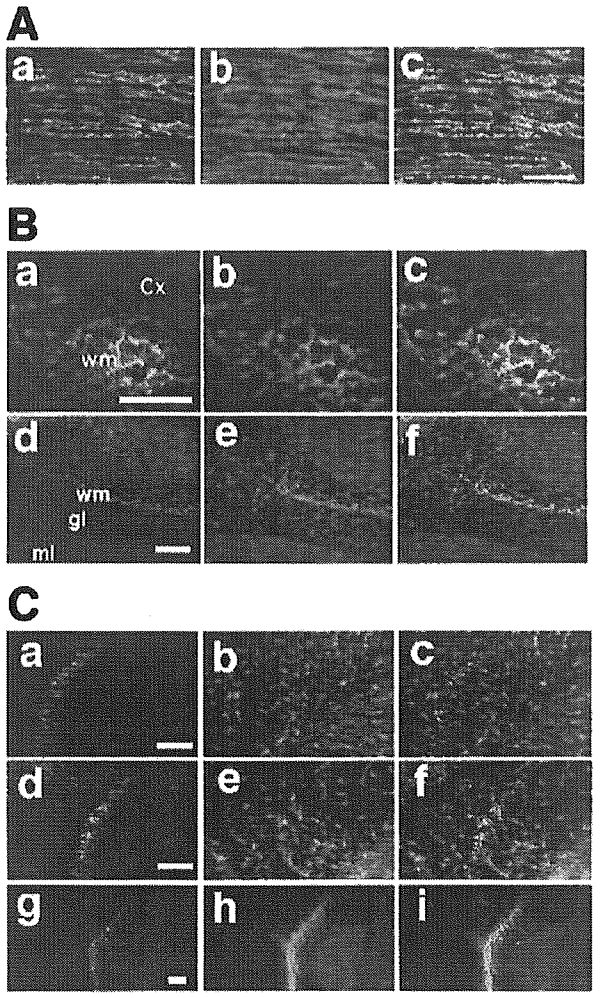

Fig. 3 – Schwann cell- and OL-specific expression of TPO1. Immunofluorescence microscopy of longitudinal sections of the mouse sciatic nerve (A; paraffin; 5 μm thickness), cerebrum (Ba–c) and cerebellum (Bd–f) (frozen section; 20 μm thickness). A and B show staining results as follows: anti-TPO1 (ABEP05; green, A-a and B-a and B-d) and anti-MBP (red, A-b and B-b and B-e). Merged images are shown in A-c and B-c and B-f. Scale bar = 40 μm in A and 50 μm in B. (C) Immunofluorescence microscopy of cerebellum frozen sections (20 μm thickness) stained with neuronal or glial cell markers: anti-TPO1 (ABEP05; a, d and g) and anti-Map2 for neurons (b), anti-GFAP for astrocytes (e), and O4 for OLs (h). Merged images are indicated on the extreme right of each row (c, f and i). Images were obtained by confocal microscopy. Scale bars = 50 μm. Cx, cortex; ml, molecular cell layer; gl, granule cell layer; wm, white matter.

2.9. *MAG cross-linking-induced assembly of TPO1 protein*

Cross-linking of cell surface MAG by a MAG-specific antibody is known to induce tyrosine phosphorylation of Fyn; moreover, the MAG–Fyn pathway is involved in the initial events of myelination (Umemori et al., 1994). To examine whether TPO1 is involved in the MAG–Fyn pathway, we performed a MAG cross-linking experiment in OL-lineage cells. Small dot-like TPO1 signals increased within 30 min in immature OLs treated with anti-MAG IgG (Fig. 8A) in comparison with control IgG (Fig. 8B). Quantitative analysis showed that the number of TPO1-immunoreactive dot-like signals significantly increased by twofold in MAG cross-linked immature OLs (anti-MAG IgG = 136.9 ± 18.73 vs. control IgG = 67.9 ± 8.35, $P < 0.001$, $n = 21$ cells; Fig. 8C). These results suggested that MAG cross-linking altered TPO1 localization via oligomerization of cell surface MAG and that TPO1 is involved in MAG-mediated signaling.

3. Discussion

We have characterized the distribution of TPO1, a new myelin membrane protein of the AIGP family. Previous studies have analyzed expression of the TPO1 gene (Krueger et al., 1997). However, the precise distribution of the protein has not been defined due to the lack of suitable TPO1-specific antibodies, probably because this protein is extremely hydrophobic (average hydrophobicity = 0.39, calculated by the Kyte and

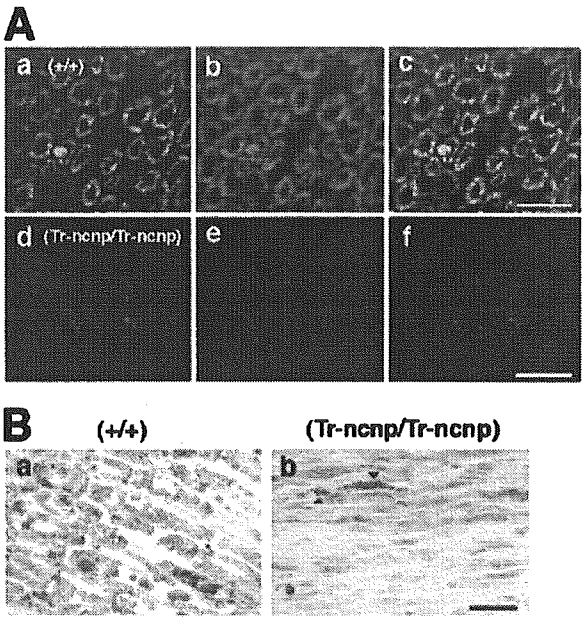

Fig. 4 – Altered expression pattern of TPO1 in the sciatic nerves of trembler mice. (A) Transverse sections (paraffin; 5 μm thickness) of sciatic nerves from adult wild-type (upper images) or trembler-Ncnp mice (lower images). MBP (b, e) was used as a myelin membrane marker in double-labeling experiments with anti-TPO1 (ABEP05; a, d). Merged images are shown in c and f. TPO1 staining in the sciatic nerves was detected in Schwann cell myelin membranes and was decreased in trembler mice. Images were obtained using a CCD camera. Scale bars = 40 μm. (B) Longitudinal section of sciatic nerves from adult wild-type (left) or trembler mice (right). Sections (paraffin; 5 μm thickness) were stained with anti-TPO1 (ABEP05) and were visualized with diaminobenzidine (DAB) and methylene blue for nuclei. TPO1-positive aggregates were observed (b, arrowhead). Scale bars = 20 μm.

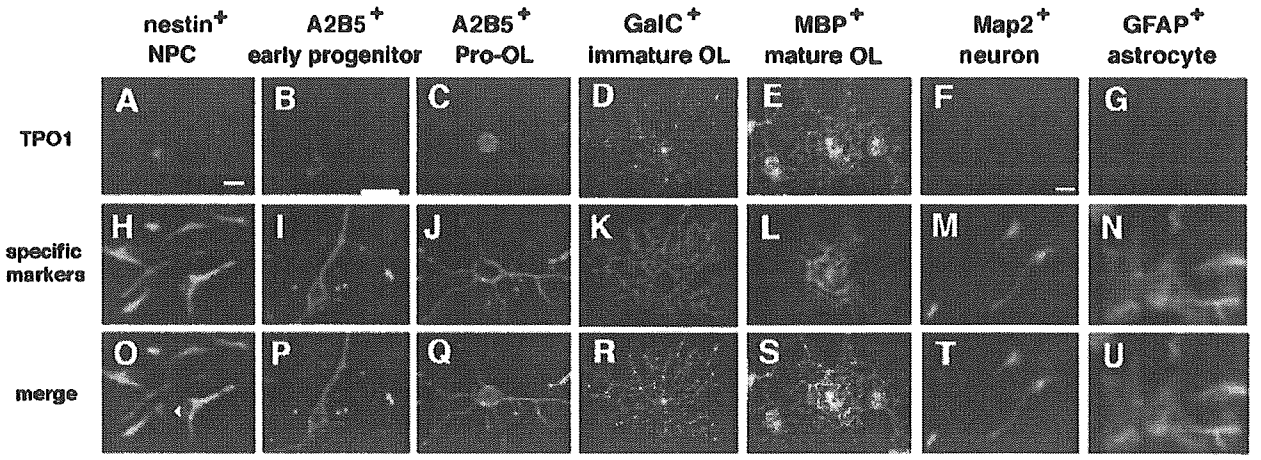

Fig. 5 – TPO1 is specifically expressed in OL lineage cells. TPO1 expression was evaluated in isolated CNS cells. Panels A, H and O: Neuroepithelial cells prepared from E14 mouse cortex. Panels B–E, I–L and P–S: OL lineage cells from P7 rat optic nerves. OPCs were cultured in differentiation medium for 6 hr (for early progenitors: B, I and P), 2 days (for Pro-OLs: C, J and Q), 4 days (for immature OLs: D, K and R) or 6 days (for mature OLs: E, L and S). Panels F, M and T: Primary cultured neurons were prepared from E14 mouse cortex. Panels G, N and U: Astrocytes from P1 mouse cortex. These cells were immunostained with anti-TPO1 (A–G) and anti-nestin (H), A2B5 (I and J), GalC (K), anti-MBP (L), anti-Map-2 (M) or anti-GFAP (N). Merged images are presented in panels O–U. Images A, H and O and F, G, M, N, T and U were obtained with a cooled CCD camera. Images B–E, I–L and P–S were obtained with a confocal laser microscope. Scale bars = 25 μm in A, F, G, H, M–O, T and U, and 20 μm in B–E, I–L and P–S.

Doolittle method (Kyte and Doolittle, 1982). In this work, we generated TPO1-specific antibodies and showed that TPO1 specifically distributes to the myelin membrane of Schwann cells and OLs and colocalizes with Fyn and GalC in cultured OLs. Our analyses suggested that TPO1 function may possibly be linked to the autophosphorylation of Fyn in the myelin membrane.

Phylogenetic analysis showed that TPO1 has diverged from AIGP1 and TMS2 (Fig. 1A). According to this evolutionary classification, the expression patterns of AIGP-family members in nervous systems have been divided into two groups: AIGP1 and TMS-2, which are expressed in neurons (Grossman et al., 2000; Aoki et al., 2002), and TPO1, which is expressed specifically in OLs and Schwann cells. Highly organized compact myelin is unique to vertebrates (Baumann and Pham-Dinh, 2001), thus *Drosophila melanogaster* lacks compact myelin and has only one AIGP family member, dTMS (Grossman et al., 2000), which is more similar to AIGP1 than TPO1 (Fig. 1A). These facts suggest that the evolutionary origins of compact myelin in vertebrates involved the emergence of the TPO1 gene and that TPO1 may play an important role in the formation and maintenance of compact myelin in vertebrates.

Trembler mice lack compact myelin in the PNS. The trembler phenotype is caused by an inherited mutation in the PMP22 gene (Suter et al., 1992; Suh et al., 1997; Sakai et al., 1999). The expression of the myelin membrane proteins P0, MBP and MAG is significantly reduced in the PNS, and the localization pattern of MAG is altered in Schwann cells of trembler mice (Vallat et al., 1999). In the present study, immunohistochemical analysis revealed that TPO1 expression is significantly reduced in the PNS myelin membrane of trembler-Ncnp mice, indicating that TPO1 is a myelin membrane protein. Furthermore we found that the localization pattern of TPO1 is altered in Schwann cells of the trembler mouse, and this altered pattern is similar to that of MAG in the trembler mouse (Vallat et al., 1999), suggesting a possible link between TPO1 and MAG in myelin formation and maintenance.

In the developing rodent brain, the proliferation of OL progenitors increases after birth. Myelin formation starts around P0 and largely occurs between P10 and P60 (Baumann and Pham-Dinh, 2001). The TPO1 gene expression is markedly upregulated from P10 to P20, an early phase of active myelination (Fig. 2). During this stage, immature OLs contact axons and transform into MBP(+) mature OLs. Previous studies have indicated that neuronal contact leads to the activation of PLP, MBP and MAG genes in OLs in vivo and in vitro (Macklin et al., 1986; Kidd et al., 1990; Matsuda et al., 1997). Together with its OL-specific localization, the expression profile of TPO1 in the developing brain suggests that the upregulation of gene expression in P10–20 mice may be triggered by neuron–OL interactions, which in turn may be involved in the induction of myelination. Thus, it is important to further elucidate the relationship between TPO1 and neuron–OL interaction.

Immunofluorescence analyses with organelle-specific markers showed that TPO1 localizes to Golgi in OL cell bodies. Previous experiments demonstrated that another family member, AIGP1, is similarly localized to the Golgi in neurons (Aoki et al., 2002). The basis of Golgi targeting of AIGP1 and TPO1 is not known, but AIGP family members likely use a common mechanism. The known AIGP family members do not have conventional Golgi targeting signals, suggesting that these proteins contain a novel Golgi targeting mechanism. On the other hand, TPO1 also localizes to OL processes and myelin-like sheets, and the myelin protein targeting may be achieved by palmitoylation (Schneider et al., 2005). The localization of TPO1 partially overlapped with that of Fyn,

which is also a palmitoylated protein (Shenoy-Scaria et al., 1993; Koegl et al., 1994; Wolven et al., 1997). Protein palmitoylation is a post-translational lipid modification that mediates interactions with cellular membranes (Han and Martinage, 1992; Koegl et al., 1994) and recruits multiple classes of signaling molecules to specialized membrane microdomains

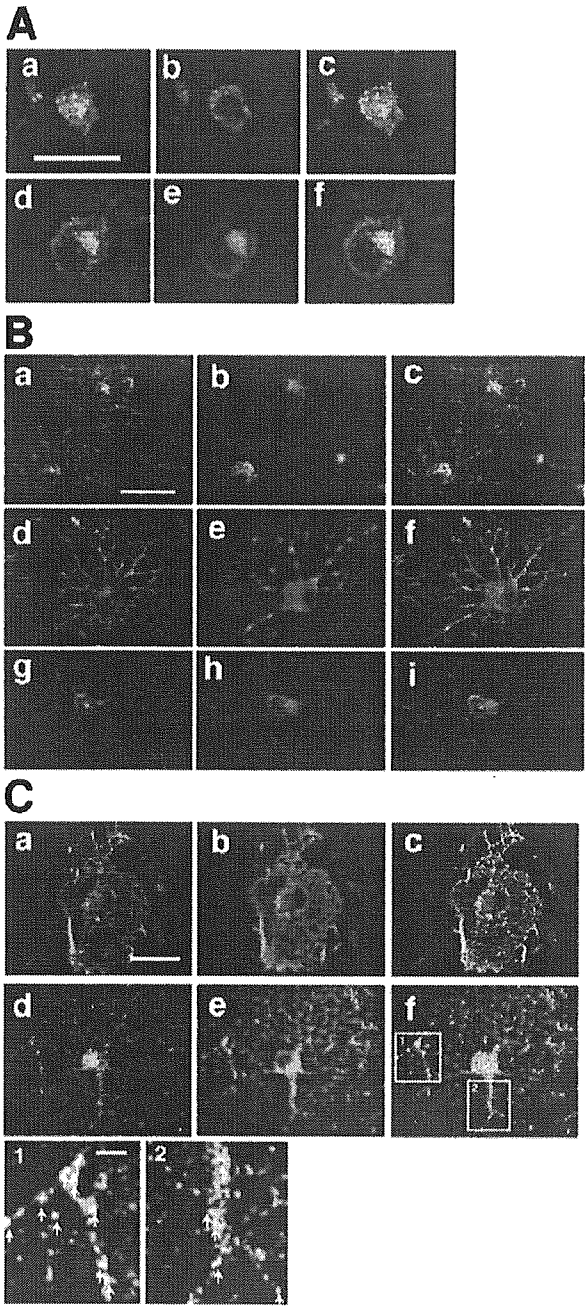

Fig. 6 – Subcellular localization of TPO1 in OLs. OPCs derived from rat optic nerve were cultured in differentiation medium for 6 days. Mature OLs with cell processes and myelin-like membrane sheets were double-stained with anti-TPO1 (A-a and A-d; B-a, B-d and B-g; and C-a, C-d and C-g) and the following organelle markers: anti-KDEL (endoplasmic reticulum; Ab), anti-GM130 (Golgi; Ae), anti-Lamp-1 (late endosomes and lysosomes; B-b), anti-Rab3a (secretory vesicles; B-e) and anti-EEA1 (early endosomes; B-h). Merged images are presented in A-c and A-f, and B-c, B-f and B-i. Images were obtained by confocal microscopy; scans through the cell bodies (A) and cell processes and myelin-like membrane sheets (B) are shown. Scale bars = 20 μm. (C) OLs with multiple cell processes (a–c) and myelin-like sheets (d–i) were double-stained with anti-TPO1 (a and d) and anti-GalC (b) or anti-Fyn (e). Merged images are presented in panels c and f. Images in region 1 and 2 of panel f were magnified and are presented in panels 1 and 2, respectively. Arrows in 1 and 2 indicate overlapping signals (yellow). Images were obtained by confocal microscopy. Scale bar (a) = 20 μm, Scale bar (1) = 5 μm.